

19. N. Knowles, M. D. Dettinger, D. R. Cayan, *J. Clim.* **19**, 4545 (2006).
20. P. W. Mote, A. F. Hamlet, M. P. Clark, D. P. Lettenmaier, *Bull. Am. Meteorol. Soc.* **86**, 39 (2005).
21. I. T. Stewart, D. R. Cayan, M. D. Dettinger, *J. Clim.* **18**, 1136 (2005).
22. A. L. Westerling, H. G. Hidalgo, D. R. Cayan, T. W. Swetnam, *Science* **313**, 940 (2006); published online 5 July 2006 (10.1126/science.1128834).
23. N. McDowell et al., *New Phytol.* **178**, 719 (2008).
24. C. Bigler, D. G. Gavin, C. Gunning, T. T. Veblen, *Oikos* **116**, 1983 (2007).
25. A. W. Fellows, M. L. Goulden, *Geophys. Res. Lett.* **35**, L12404 (2008).
26. We thank the many people involved in establishing and maintaining the permanent forest plots; C. Allen, A. Das, J. Halofsky, J. Hicke, J. Lutz, and four anonymous reviewers for helpful comments on the manuscript; and J. Yee for essential statistical advice. The forest plots were funded by NSF's Long-term Studies Program (DEB-0218088); the Wind River Canopy Crane Program through cooperative agreement PNW 08-DG-11261952-488 with the USDA Forest Service Pacific Northwest Research Station; various awards through the USDA Forest Service's Pacific Northwest, Pacific Southwest, and Rocky Mountain research stations and the McIntire-Stennis Cooperative Forestry Program; NSF awards DEB-0743498 and BCS-0825823; the Natural Science and Engineering Research Council of Canada;

and various awards through the U.S. National Park Service and U.S. Geological Survey (USGS). This work is a contribution of the Western Mountain Initiative (a USGS global change research project) and the Cordillera Forest Dynamics Network (CORFOR).

Supporting Online Material

www.sciencemag.org/cgi/content/full/323/5913/521/DC1
 Materials and Methods
 SOM Text
 Figs. S1 to S6
 Tables S1 to S4
 References

22 August 2008; accepted 3 December 2008
 10.1126/science.1165000

The Sphingolipid Transporter Spns2 Functions in Migration of Zebrafish Myocardial Precursors

Atsuo Kawahara,^{1,2*} Tsuyoshi Nishi,^{3,4} Yu Hisano,^{3,4} Hajime Fukui,¹ Akihito Yamaguchi,^{3,4} Naoki Mochizuki¹

Sphingosine-1-phosphate (S1P) is a secreted lipid mediator that functions in vascular development; however, it remains unclear how S1P secretion is regulated during embryogenesis. We identified a zebrafish mutant, *ko157*, that displays cardia bifida (two hearts) resembling that in the *S1P receptor-2* mutant. A migration defect of myocardial precursors in the *ko157* mutant is due to a mutation in a multipass transmembrane protein, *Spns2*, and can be rescued by S1P injection. We show that the export of S1P from cells requires *Spns2*. *spns2* is expressed in the extraembryonic tissue yolk syncytial layer (YSL), and the introduction of *spns2* mRNA in the YSL restored the cardiac defect in the *ko157* mutant. Thus, *Spns2* in the YSL functions as a S1P transporter in S1P secretion, thereby regulating myocardial precursor migration.

During the late stages of zebrafish segmentation characterized by the formation of the somites, the myocardial precursors from both sides of the anterior lateral plate mesoderm migrate toward the midline to form the heart tube (1, 2). Forward genetic analysis in zebrafish has helped to uncover genes involved in vertebrate heart formation (3). To identify additional regulators of heart development, we performed *N*-ethyl-*N*-nitrosourea (ENU) mutagenesis screening for mutations specifically affecting cardiac morphogenesis. We isolated a recessive *ko157* mutant that displayed two hearts, a condition known as cardia bifida with swollen pericardial sacs (Fig. 1, A, B, E, and F). The expression of myocardial markers [*nkx2.5* and cardiac myosin light chain 2 (*cmlc2*)] and chamber-specific markers [atrial myosin heavy chain (*amhc*) and ventricular myosin heavy chain (*vmhc*)] was de-

tected in two separated domains (Fig. 1, C and G, and fig. S2); this finding suggests that the myocardial precursors failed to migrate but differen-

tiated into two chambers at the bilateral positions. The migration of several mesodermal derivatives examined by the expression pattern of a vascular marker (*flil*), an erythroid marker (*gata1*), a pronephric marker (*pax2*), and a lateral plate mesoderm marker (*hand2*) was not impaired in *ko157* mutants (figs. S2 and S3), which suggests that the migration of myocardial precursors is dominantly affected. Besides cardia bifida, there were abnormal blisters at the tip of the tail in the mutant (Fig. 1, D and H). These two characteristic phenotypes (cardia bifida and tail blisters) in the *ko157* mutant were similar to those in the *miles apart* (*mil*)/*S1P receptor-2* (*S1P2*) mutant (4). Sphingosine-1-phosphate (S1P) is a lipid mediator involved in cell growth, death, migration, and differentiation (5–8). Both cardia bifida and tail blisters were observed in embryos injected with an antisense morpholino for *mil/S1P2* (*mil* MO; 15 ng) (9) (fig. S4 and table S1), suggesting a genetic interaction between *ko157* and *mil/S1P2*.

Genetic mapping of the *ko157* mutation by means of simple sequence length polymorphism

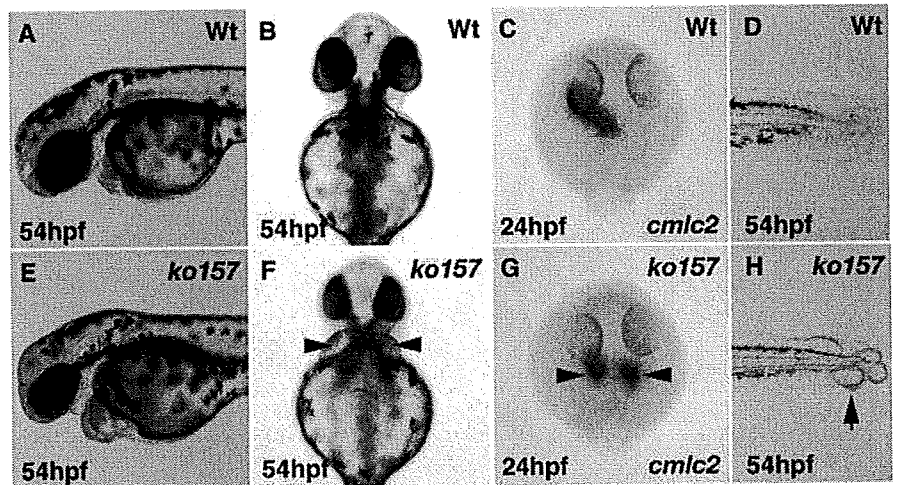


Fig. 1. Morphological phenotypes of *ko157* mutants. (A, B, D, E, F, and H) Stereomicroscopic views of wild-type (Wt) embryo [(A), (B), and (D)] and *ko157* mutant [(E), (F), and (H)]. Two swollen pericardial sacs (arrowheads) at 54 hours post-fertilization (hpf) were observed in *ko157* mutant [(E) and (F)] but not in Wt embryos [(A) and (B)]. (B) and (F) are ventral views. (C and G) Two hearts (arrowheads) in *ko157* mutants at 24 hpf were visualized (dorsal view) by whole-mount in situ hybridization with antisense *cmlc2* probe. *ko157* mutant (H), but not Wt embryos (D), exhibited tail blisters (arrow).

¹Department of Structural Analysis, National Cardiovascular Center Research Institute, Fujishirodai 5-7-1, Suita, Osaka 565-8565, Japan. ²HMRO, Kyoto University Faculty of Medicine, Yoshida, Sakyo-Ku, Kyoto 606-8501, Japan. ³Department of Cell Membrane Biology, Institute of Scientific and Industrial Research, Osaka University, 8-1 Mihogaoka, Ibaraki-shi, Osaka 567-0047, Japan. ⁴Graduate School of Pharmaceutical Sciences, Osaka University, Suita-shi, Osaka 565-0871, Japan.

*To whom correspondence should be addressed. E-mail: atsuo@ri.ncvc.go.jp

(SSLP) markers revealed that the locus of *ko157* was very close to z9419 and z63525 on linkage group 5 (Fig. 2A). We found that the *ko157* mutant allele contained a point mutation in the *spns2* gene with a substitution of arginine to serine at amino acid position 153 (R153S). This arginine is conserved between zebrafish Spns2 and mammalian homologs of Spns2 (fig. S5). Spns1

is a member of the Spns protein family (10, 11), but injection of *spns1* MO (8 ng) into wild-type embryos did not induce cardia bifida, and injection into *ko157* embryos did not worsen the phenotype (fig. S6). Hence, Spns2, but not Spns1, is involved in cardiac morphogenesis.

To examine whether the mutation in Spns2 caused the functional impairment in *ko157* mu-

tants, we performed knockdown analysis with antisense morpholino (*spns2* MO). The *spns2* MO injection, but not control morpholino, (5-base mismatched control morpholino for *spns2* MO; 5-mis MO), suppressed the production of the mature form of *spns2* mRNA (fig. S7). Injection of *spns2* MO resulted in cardia bifida (table S1; 86%, $n = 69$) with bilateral expression of *cmlc2* (Fig. 2, B to D), with no cardia bifida in control 5-mis MO-injected embryos (table S1; 0%, $n = 68$). To evaluate whether *spns2* could rescue the *ko157* mutant phenotype, we injected *spns2* or *spns2(R153S)* (*spns2* mutant) mRNA (250 pg) into the embryos derived from *spns2^{ko157}* heterozygous carriers. Using more than 250 pg caused severe defects in the trunk and the tail as well as observation of one beating heart (fig. S8). Injection of *spns2* mRNA, but not mutant *spns2(R153S)* mRNA, effectively restored both the migration of myocardial precursors and the tail blisters (Fig. 2, E to G, fig. S9, and table S2). Injection of human *Spns2* (*hSpns2*) mRNA also rescued the cardia bifida phenotype in the *spns2^{ko157}* mutant, whereas injection of the corresponding *hSpns2* mutant, *hSpns2(R199S)*, did not (fig. S10 and table S3). The *spns2^{ko157}* mutant phenotype was not restored by injection of a construct in which human Spns1 is fused to enhanced green fluorescent protein (EGFP), *hSpns1-EGFP* (fig. S10 and table S3). These results show that Spns2 function is conserved from fish to mammals and that Spns1 cannot compensate for the loss of Spns2.

Because the cardia bifida phenotype in the *spns2^{ko157}* mutant was similar to that in the *mil/S1P2* mutant, we investigated a possible genetic interaction between *spns2* and *mil/S1P2*. Injection of *mil* MO induced cardia bifida in embryos derived from a wild-type-*Tg(cmlc2:mRFP)* cross in a dose-dependent manner (table S1, *mil* MO 15-ng injection; 90%, $n = 49$; table S4, *mil* MO

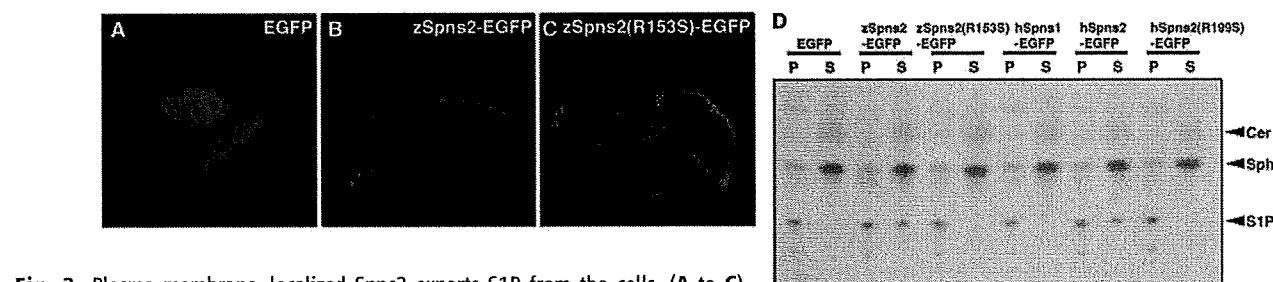
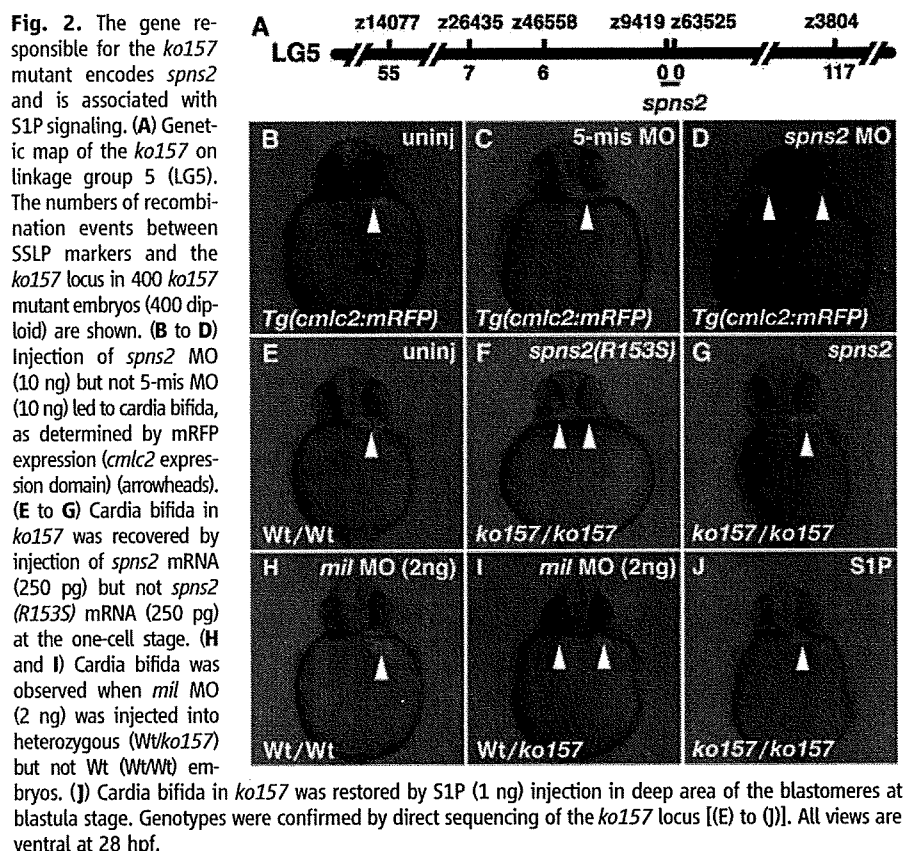


Fig. 3. Plasma membrane-localized Spns2 exports S1P from the cells. (A to C) Confocal fluorescence microscopy images of CHO cells expressing mouse SphK1 transfected with the plasmids indicated. (D) [³H]S1P converted from [³H]sphingosine in the lipids extracted from medium (S, supernatant) and cells (P, pellet) was separated on a thin-layer chromatography plate. Cer, Sph, and S1P indicate the positions of [³H]ceramide, [³H]sphingosine, and [³H]S1P, respectively. (E) Relative amount of secreted S1P indicates the percentage of total [³H]S1P (P + S). Data are expressed as means ± SD of more than three independent experiments of (D).

2-ng injection; 7%, $n = 55$). Low-dose *mil* MO (2 ng) injections in *spns2^{ko157}* heterozygous embryos resulted in a higher frequency of cardia bifida relative to wild-type embryos (table S4; 44%, $n = 18$). Genotyping revealed that most cardia bifida embryos were wild-type/*ko157* (Fig. 2, H and I, and table S4). The severity of the cardiac defect was comparable between *mil* MO (15 ng)-injected wild-type and *mil* MO-injected *ko157* embryos (fig. S11). These data suggest that *spns2* genetically interacts with *mil/SIP2*.

To further examine the functional interaction of Spns2 and SIP signaling, we performed a rescue experiment of the *spns2^{ko157}* mutant by SIP injection. When SIP (1 ng) was injected deep into an area of the blastomeres of blastula-stage embryos derived from *spns2^{ko157}* heterozygous carriers, cardia bifida was effectively restored (Fig. 2J and table S2). In addition, the cardia bifida phenotype induced by *mil* MO (15 ng) injection into the yolk was not rescued by subsequent injection of *spns2* mRNA (250 pg) into the blastomere of one- to two-cell-stage embryos (fig. S12), which suggests that Spns2 functions upstream of Mil/SIP₂ (fig. S1).

The putative 12-transmembrane domains, together with the predicted structural similarity between zebrafish Spns2 (zSpns2) and the bacterial glycerol-3-phosphate transporter (12) and the genetic interaction of Spns2 and the SIP-mediated signaling, suggested that Spns2 might function as a SIP transporter. To test this, we used Chinese hamster ovary (CHO) cells expressing a sphingosine kinase, *mSphK1*, essential for SIP synthesis (CHO-SphK cells) (fig. S1). Although [³H]sphingosine was taken up by the cells and effectively converted to [³H]SIP, it was not secreted because of the absence of an SIP export activity. We examined whether the expression of zSpns2-EGFP or zSpns2(R153S)-EGFP was able to induce SIP export. Both zSpns2-EGFP and zSpns2(R153S)-EGFP were predominantly localized within the plasma membrane and in the endosomes of transfected CHO-SphK cells (Fig. 3, A to C), consistent with a role in membrane trafficking. Expression of zSpns2-EGFP resulted in a time-dependent export of [³H]SIP that was not seen in either the EGFP- or zSpns2(R153S)-EGFP-transfected cells (Fig. 3, D and E, and fig. S13). Moreover, endogenous SIP release was also detected only in the medium from the zSpns2-EGFP-expressing cells (fig. S14) without altering the content of cellular sphingolipids (fig. S15). Overexpression of hSpns2-EGFP enhanced SIP export to a similar extent as zSpns2-EGFP, whereas that of hSpns2(R199S)-EGFP and hSpns1-EGFP did not (Fig. 3, D and E). SIP release was not due to cell death induced by Spns2-EGFP expression (fig. S16), and the activity of sphingosine kinase in the medium was not affected by Spns2-EGFP expression (fig. S17).

Recently it was proposed that ABC transporters including ABCC1 and ABCA1 are required for SIP transport (13–15). The cellular distribution of Spns2-EGFP is similar to that of ABCA1

(16). Therefore, the net SIP release to the outside of the cells would depend on the amount of Spns2 and other SIP transporters expressed on the plasma membrane. The contribution of ABC transporters in the SIP transport is still controversial in vivo because the quantity of plasma SIP is not altered in mice deficient for ABCC1 or ABCA1 (17). We propose that Spns2 is a SIP transporter essential for the SIP-mediated signaling pathway in vivo (fig. S1).

To further understand where and how Spns2 functions in vivo, we examined *spns2* expression during early embryogenesis by whole-mount in situ hybridization. The expression of *spns2* was induced at the marginal cells of the blastoderm at dome stage (fig. S18). During gastrulation stages, *spns2* was predominantly expressed in the extraembryonic yolk syncytial layer (YSL) with a dorsal-to-ventral gradient (Fig. 4A and fig. S18). *spns2* expression in the YSL was strongly detected just below the developing myocardial precursors and was maintained throughout the segmentation period (Fig. 4, B to D). Recent evidence demonstrated that both endoderm and YSL regulate cardiac morphogenesis (18–20). Expression of the endoderm markers *sox17* and *foxa2* was not affected in *spns2^{ko157}* mutant em-

bryos (fig. S3). In addition, *spns2* expression was not affected in endoderm-defective *casanova/sox32* morphants (fig. S18), which suggests that *spns2* expression in the YSL is regulated independently of the endoderm. *spns2* expression was detected in somites and in the tip of the tail at the 15-somite stage (fig. S18). We observed *spns2* expression in the myocardial precursors and in the intermediate cell mass (fig. S18). Thus, the expression of *spns2* is complex and dynamic. Although the overall morphology of the head and trunk appeared to be normal in the *spns2^{ko157}* mutant, we observed substantially increased apoptotic cells in the tail but not in the heart, head, and anterior trunk of the *spns2^{ko157}* mutant (fig. S19). These results suggest the involvement of Spns2 in the regulation of multiple organogenesis processes.

Because *spns2* was strongly expressed in the YSL below the developing myocardial precursors, we further examined whether Spns2 in the YSL contributes to the migration of myocardial precursors. When *spns2* MO (10 ng) was injected into the YSL at shield stage, cardia bifida was observed (Fig. 4, E and F, and table S5). In contrast, *mil* MO (15 ng) injection in the YSL at shield stage did not induce cardia bifida (Fig. 4,

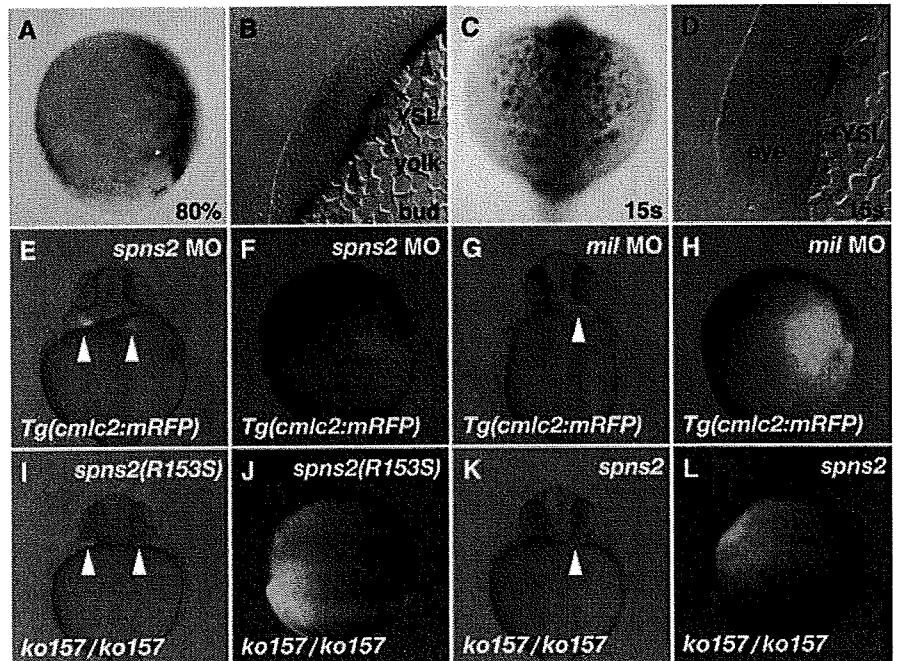


Fig. 4. Spns2 in the YSL is required for the migration of myocardial precursors. (A to D) Whole-mount in situ hybridization with antisense *spns2* probe at different stages of development. (B) and (D) show transverse sections of *spns2*-stained embryos. *spns2* was expressed in the YSL with a dorsal-to-ventral gradient at 80% epiboly stage [(A); dorsal right, lateral view]. *spns2* expression was maintained in the YSL at bud and 15s stages [(B) and (D); red arrowheads] and detected under the anterior midline [(C); dorsal up, anterior view]. (E to H) Injection of *spns2* MO (10 ng) with fluorescein isothiocyanate (FITC)-dextran into the YSL of shield-stage embryos led to cardia bifida, whereas injection of *mil* MO (15 ng) did not. (I to L) Cardia bifida in *spns2^{ko157}* mutant was recovered by mRNA injection of *spns2* (250 pg) with FITC-dextran into the YSL of shield-stage embryos but not by mRNA injection of *spns2(R153S)* (250 pg). Genotypes were confirmed by direct sequencing of the *ko157* locus. Injection into the YSL was confirmed by the distribution of FITC-dextran in the YSL at gastrulation stages [(F), (H), (J), and (L)]. White arrowheads indicate the positions of *cmlc2* expression domain [(E), (G), (I), and (K)].

G and H, and table S5). Because *mil/SIP2* is expressed in the mesoderm just lateral to the midline (4), *mil/SIP2* is proposed to function in mesoderm over the YSL. Further, cardia bifida in the *spns2^{ko157}* mutant was restored by the injection of *spns2* mRNA but not *spns2(R153S)* mRNA into the YSL at shield stage (Fig. 4, I to L, and table S6).

The rescue frequency by injection of *spns2* mRNA into the YSL was slightly lower than for injection into the blastomere (tables S2 and S6). One explanation is that *spns2* mRNA injected into the blastomere at the one-cell stage is widely distributed in the YSL because the YSL is constituted by marginal blastomeres collapsing onto the yolk around the 1000-cell stage. Another explanation is that the function of Spns2 in embryonic tissues as well as in the YSL may be partly required for the migration of myocardial precursors. Furthermore, transplantation analysis showed that Spns2 at least functions in a cell-nonautonomous manner, because *ko157*-derived donor cells were incorporated into single beating hearts of wild-type recipients, and wild type-derived donor cells were incorporated into one of two beating hearts of *ko157* recipients (movies S1 to S3). One attractive interpretation is that Spns2 in the YSL regulates the SIP export from the yolk to the embryonic body, leading to the activation of Mil/SIP₂ in mesoderm just lateral to the midline (fig. S1). Recent reports have pointed out the importance of *ferroportin1* (*fpn1*) as a transporter of iron from the yolk to the embryonic body (21) and the clinical relevance to hypochromic anemia and hemochromatosis in humans (22, 23).

By investigating characteristic features of the zebrafish *spns2^{ko157}* mutant and analyzing the biological activity of Spns2, we have demonstrated that Spns2 functions as a SIP transporter and that Spns2 in the extraembryonic YSL is a prerequisite for the migration of myocardial precursors, presumably mediated by the SIP-Mil/SIP₂ pathway. The identification of Spns2 not only contributes to our understanding of the molecular mechanism of biological SIP delivery, but may also elucidate the physiological importance of Spns2 in autoimmune disease (24), cardiovascular diseases, and cancer (25) in which SIP plays a central role.

References and Notes

1. D. Y. Stainier, *Nat. Rev. Genet.* **2**, 39 (2001).
2. J. J. Schoenebeck, D. Yelon, *Semin. Cell Dev. Biol.* **18**, 27 (2007).
3. J. N. Chen, M. C. Fishman, *Trends Genet.* **16**, 383 (2000).
4. E. Kupperman, S. An, N. Osborne, S. Waldron, D. Y. Stainier, *Nature* **406**, 192 (2000).
5. M. J. Lee *et al.*, *Science* **279**, 1552 (1998).
6. T. Hla, *Pharmacol. Res.* **47**, 401 (2003).
7. S. Spiegel, S. Milstien, *Nat. Rev. Mol. Cell Biol.* **4**, 397 (2003).
8. Y. A. Hannun, L. M. Obeid, *Nat. Rev. Mol. Cell Biol.* **9**, 139 (2008).
9. T. Matsui *et al.*, *Nat. Clin. Pract. Cardiovasc. Med.* **4** (suppl. 1), 577 (2007).
10. Y. Nakano *et al.*, *Mol. Cell Biol.* **21**, 3775 (2001).
11. R. M. Young *et al.*, *Dev. Dyn.* **223**, 298 (2002).
12. Y. Huang, M. J. Lemieux, J. Song, M. Auer, D. N. Wang, *Science* **301**, 616 (2003).
13. N. Kobayashi *et al.*, *J. Lipid Res.* **47**, 614 (2006).
14. P. Mitra *et al.*, *Proc. Natl. Acad. Sci. U.S.A.* **103**, 16394 (2006).
15. K. Sato *et al.*, *J. Neurochem.* **103**, 2610 (2007).
16. E. B. Neufeld *et al.*, *J. Biol. Chem.* **276**, 27584 (2001).
17. Y. M. Lee, K. Venkataraman, S. I. Hwang, D. K. Han, T. Hla, *Prostaglandins Other Lipid Mediat.* **84**, 154 (2007).

18. Y. Kikuchi *et al.*, *Genes Dev.* **15**, 1493 (2001).
19. T. Dickmeis *et al.*, *Genes Dev.* **15**, 1487 (2001).
20. T. Sakaguchi, Y. Kikuchi, A. Kuroiwa, H. Takeda, D. Y. Stainier, *Development* **133**, 4063 (2006).
21. A. Donovan *et al.*, *Nature* **403**, 776 (2000).
22. O. T. Njajou *et al.*, *Nat. Genet.* **28**, 213 (2001).
23. G. Montosi *et al.*, *J. Clin. Invest.* **108**, 619 (2001).
24. M. Sekiguchi *et al.*, *J. Immunol.* **180**, 1921 (2008).
25. S. Milstien, S. Spiegel, *Cancer Cell* **9**, 148 (2006).
26. We thank M. Sone and M. Minamimoto for technical assistance; S. Endo and R. Hanaoka for the mutagenesis screening; T. Kitaguchi for the establishment of *cmc2:mRFP*; M. Masuda, Y. Igarashi, A. Kihara, S. Mitsutake, K. Shiota, I. B. David, and Y. Kaziro for support and suggestions; M. Hibi, J. S. Gutkind, and M. Tsang for critical reading and valuable suggestions; D. Y. Stainier for discussions and sharing of unpublished data; and H. Okamoto, K. Kawakami, Y. Kikuchi, H. Yanagisawa, D. Yamamoto, R. Y. Tsien, and H.-J. Tsai for fish and reagents. Supported by grants from the Ministry of Education, Culture, Sports, Science and Technology of Japan; the National BioResource Project of Japan; the Japan Society for the Promotion of Science; the Program for the Promotion of Fundamental Studies in Health Sciences of the National Institute of Biomedical Innovation; the Ministry of Health, Labor and Welfare of Japan; and the Takeda Science Foundation. The sequences of zebrafish *spns2*, human *Spns2*, and mouse *Spns2* have been deposited in the DNA Data Bank of Japan [accession numbers: AB441164 (zebrafish), AB441165 (human), AB441166 (mouse)]. The authors are filing a patent based on the results reported in this paper.

Supporting Online Material

www.sciencemag.org/cgi/content/full/1167449/DC1

Materials and Methods

Figs. S1 to S19

Tables S1 to S6

Movies S1 to S3

References

20 October 2008; accepted 3 December 2008

Published online 11 December 2008;

10.1126/science.1167449

Include this information when citing this paper.

The Peopling of the Pacific from a Bacterial Perspective

Yoshan Moodley,^{1*†} Bodo Linz,^{1*‡} Yoshio Yamaoka,^{2*} Helen M. Windsor,³ Sebastien Breurec,^{4,5} Jeng-Yih Wu,⁶ Ayas Maady,⁷ Steffie Bernhöft,¹ Jean-Michel Thiberge,⁸ Suparat Phanukoonon,⁹ Gangolf Jobb,¹⁰ Peter Siba,⁹ David Y. Graham,² Barry J. Marshall,³ Mark Achtman^{1,11,§}

Two prehistoric migrations peopled the Pacific. One reached New Guinea and Australia, and a second, more recent, migration extended through Melanesia and from there to the Polynesian islands. These migrations were accompanied by two distinct populations of the specific human pathogen *Helicobacter pylori*, called hpSahul and hspMaori, respectively. hpSahul split from Asian populations of *H. pylori* 31,000 to 37,000 years ago, in concordance with archaeological history. The hpSahul populations in New Guinea and Australia have diverged sufficiently to indicate that they have remained isolated for the past 23,000 to 32,000 years. The second human expansion from Taiwan 5000 years ago dispersed one of several subgroups of the Austronesian language family along with one of several hspMaori clades into Melanesia and Polynesia, where both language and parasite have continued to diverge.

After modern humans dispersed “out of Africa” about 60,000 years ago (60 ka) (1), they reached Asia via a southern coastal route (2). That route extended along the Pleistocene landmass, known as Sundaland (i.e., the Malay peninsula, Sumatra, Java, Borneo, and

Bali), that was joined to the Asian mainland as a result of low sea levels during the last ice age (12 to 43 ka) (3). Low sea levels also meant that Australia, New Guinea, and Tasmania were connected in a continent called Sahul, separated from Sundaland by a few narrow deep-sea channels. It

seems Sahul was colonized only once, ~40 to 50 ka (3, 4), although backed-blade stone tool technology and the dingo appear to have been introduced from India at a later date (5, 6).

¹Max-Planck-Institut für Infektionsbiologie, Department of Molecular Biology, Charitéplatz 1, 10117 Berlin, Germany. ²Department of Medicine-Gastroenterology, Baylor College of Medicine and Michael E. DeBakey VA Medical Center, Houston, TX 77030, USA. ³Microbiology and Immunology M502, School of Biomedical, Biomolecular and Chemical Sciences, University of Western Australia, Australia 6009. ⁴Institut Pasteur, BP 220, Dakar, Sénégal. ⁵Institut Pasteur de Nouvelle-Calédonie, BP61, 98845 Noumea, New Caledonia. ⁶Department of Gastroenterology, Kaohsiung Medical University, 100 Shih-Chuan 1st Road, Kaohsiung 80708, Taiwan. ⁷Department of Endoscopy, Republic Hospital No. 1, Kyzyl City 667003, Republic of Tuva, Russia. ⁸Institut Pasteur, Genotyping of Pathogens and Public Health, 28 rue du Dr Roux, 75724 Paris, France. ⁹Papua New Guinea Institute of Medical Research, Post Office Box 60, Goroka, EHP, 441 Papua New Guinea. ¹⁰Fritz-Kortner-Bogen 36, 81739 Munich, Germany. ¹¹Environmental Research Institute and Department of Microbiology, University College Cork, Cork, Ireland.

*These authors contributed equally to this work.

†Present address: Austrian Academy of Sciences, Konrad Lorenz Institute for Ethology, Savoyenstrasse 1A, A-1160, Vienna, Austria.

‡Present address: Department of Biochemistry and Molecular Biology, Pennsylvania State University, University Park, PA 16802, USA.

§To whom correspondence should be addressed. E-mail: m.achtman@ucc.ie

Angiopoietin-like Protein 2 Promotes Chronic Adipose Tissue Inflammation and Obesity-Related Systemic Insulin Resistance

Mitsuhsa Tabata,^{1,13} Tsuyoshi Kadomatsu,¹ Shigetomo Fukuhara,⁷ Keishi Miyata,¹ Yasuhiro Ito,^{1,2} Motoyoshi Endo,¹ Takashi Urano,^{1,2} Hui Juan Zhu,¹ Hiroto Tsukano,¹ Hirokazu Tazume,¹ Koichi Kaikita,³ Kazuya Miyashita,⁸ Takao Iwawaki,⁹ Michio Shimabukuro,¹⁰ Kazuhiko Sakaguchi,¹¹ Takaaki Ito,⁵ Naomi Nakagata,⁶ Tetsuya Yamada,¹² Hideki Katagiri,¹² Masato Kasuga,^{11,16} Yukio Ando,⁴ Hisao Ogawa,³ Naoki Mochizuki,⁷ Hiroshi Itoh,¹³ Toshio Suda,¹⁴ and Yuichi Oike^{1,15,*}

¹Department of Molecular Genetics

²Department of Ophthalmology and Visual Science

³Department of Cardiovascular Medicine

⁴Department of Diagnostic Medicine

⁵Department of Pathology and Experimental Medicine

Graduate School of Medical Sciences, Kumamoto University, 1-1-1 Honjo, Kumamoto 860-8556, Japan

⁶Center for Animal Resources and Development, Kumamoto University, 2-2-1 Honjo, Kumamoto 860-0811, Japan

⁷Department of Structural Analysis, National Cardiovascular Center Research Institute, Suita, Osaka 565-8565, Japan

⁸Immuno-Biological Laboratories Co., Ltd., Aramachi, Takasaki 370-0831, Japan

⁹Initiative Research Unit, RIKEN Advanced Science Institute, Wako 351-0189, Japan

¹⁰Second Department of Internal Medicine, University of the Ryukyus, Okinawa 903-0215, Japan

¹¹Division of Diabetes, Metabolism, and Endocrinology, Department of Internal Medicine, Kobe University Graduate School of Medicine, Chuo-ku, Kobe 650-0017, Japan

¹²Division of Molecular Medicine and Diabetes, Tohoku University Graduate School of Medicine, Aoba-ku, Sendai 980-8575, Japan

¹³Division of Endocrinology, Metabolism, and Nephrology, Department of Internal Medicine

¹⁴Department of Cell Differentiation, The Sakaguchi Laboratory

School of Medicine, Keio University, Shinjuku-ku, Tokyo 160-8582, Japan

¹⁵PRESTO, Japan Science Technology Agency, Kawaguchi, Saitama 332-0012, Japan

¹⁶Present address: Research Institute, International Medical Center of Japan, Shinjuku-ku, Tokyo 162-8655, Japan

*Correspondence: oike@gpo.kumamoto-u.ac.jp

DOI 10.1016/j.cmet.2009.08.003

SUMMARY

Recent studies of obesity have provided new insights into the mechanisms underlying insulin resistance and metabolic dysregulation. Numerous efforts have been made to identify key regulators of obesity-linked adipose tissue inflammation and insulin resistance. We found that angiopoietin-like protein 2 (Angptl2) was secreted by adipose tissue and that its circulating level was closely related to adiposity, systemic insulin resistance, and inflammation in both mice and humans. Angptl2 activated an inflammatory cascade in endothelial cells via integrin signaling and induced chemotaxis of monocytes/macrophages. Constitutive Angptl2 activation *in vivo* induced inflammation of the vasculature characterized by abundant attachment of leukocytes to the vessel walls and increased permeability. Angptl2 deletion ameliorated adipose tissue inflammation and systemic insulin resistance in diet-induced obese mice. Conversely, Angptl2 overexpression in adipose tissue caused local inflammation and systemic insulin resistance in nonobese mice. Thus, Angptl2 is a key

adipocyte-derived inflammatory mediator that links obesity to systemic insulin resistance.

INTRODUCTION

Obesity is a pandemic medical and social problem that is associated with several adverse health outcomes, including type 2 diabetes, hypertension, dyslipidemia, cardiovascular disease, and cancer (Eckel et al., 2005; Mokdad et al., 2003), all of which result in increased mortality. A major metabolic manifestation of obesity is systemic insulin resistance. Recently, the concept has emerged that chronic low-grade activation of proinflammatory pathways in adipose tissue directly promotes systemic insulin resistance (Apovian et al., 2008; Neels and Olefsky, 2006; Schenk et al., 2008). Adipocytes and macrophages could be a source of several proinflammatory cytokines that activate inflammatory pathways in resident and infiltrating cells within adipose tissue in a paracrine or autocrine fashion (Kanda et al., 2006; Weisberg et al., 2006). However, the molecular mechanisms underlying inflammation of adipose tissue in obesity have not fully clarified.

Fibrinogen promotes leukocyte adhesion and cytokine secretion at sites of inflammation through integrin-dependent inflammatory pathways (Herrick et al., 1999; Mosesson, 2005).

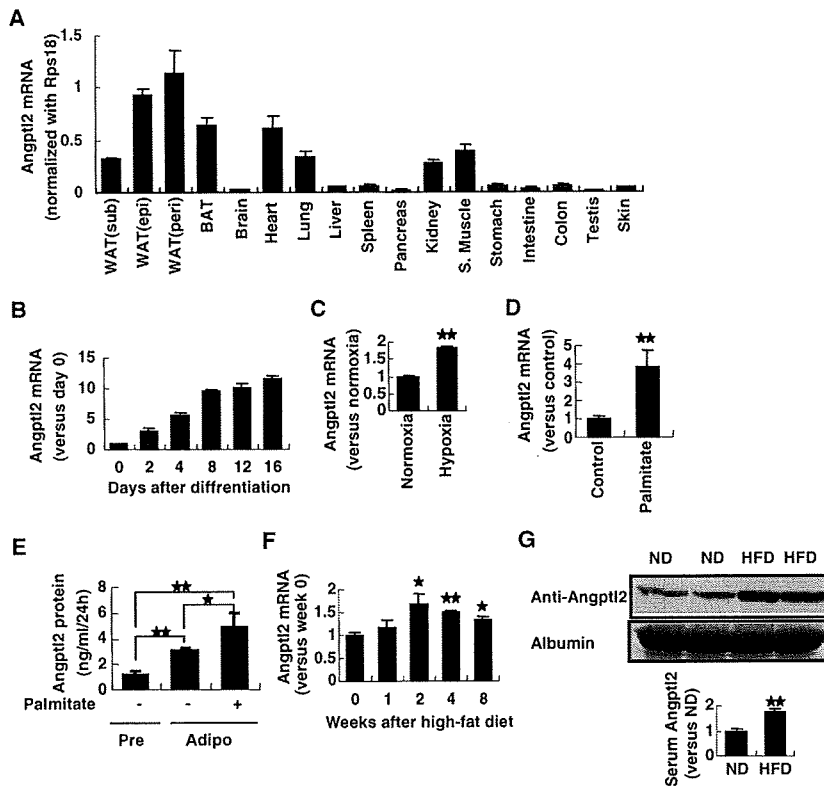


Figure 1. Angptl2 Is Secreted by Adipose Tissue

(A) Angptl2 mRNA expression in various tissues of mice fed normal chow (n = 4). WAT, white adipose tissue; sub, subcutaneous; peri, perirenal; mes, mesenteric; BAT, brown adipose tissue; S. Muscle, skeletal muscle.

(B–D) Angptl2 mRNA expression in 3T3-L1 cells during adipocyte differentiation (n = 3) (B), in differentiated 3T3-L1 cells incubated under hypoxic conditions (1% O₂, 24 hr, n = 3) (C), and in cells treated with palmitate (200 μM, 24 hr, n = 4) (D).

(E) Angptl2 protein levels in culture medium of pre- (Pre) or postdifferentiated (Adipo) 3T3-L1 cells with or without palmitate treatment (200 μM, 24 hr, n = 4).

(F) Angptl2 mRNA expression in the mesenteric adipose tissue of obese mice fed a high-fat diet for the indicated periods starting at 8 weeks of age (n = 4).

(G) Representative western blot and quantitative evaluation of serum Angptl2 protein in mice fed a normal diet (ND) or a high-fat diet (HFD) for a period of 8 weeks (n = 4). CBB-stained albumin is as control bands for protein loading. Data are the mean ± SEM, *p < 0.05 and **p < 0.01 compared with controls.

Fibrinogen-binding integrins are abundantly expressed by monocytes/macrophages and endothelial cells, and fibrinogen must undergo oligomerization or polymerization to display its activity. The presence of extravascular fibrinogen at sites of inflammation has been documented by pathologists for decades (Dvorak et al., 1985). These findings prompted us to ask whether an oligomeric protein derived from adipose tissue and containing a fibrinogen-like sequence might play a pathological role in inflammatory changes of adipose tissue associated with obesity. Recently, we and others identified seven angiopoietin-like proteins (Angptl1s), which possess a coiled-coil domain at the N terminus for oligomerization and a C-terminal fibrinogen-like domain (Kim et al., 1999; Kubota et al., 2005a; Oike et al., 2004). Angptl1s are structurally similar to Tie-2 receptor ligands (angiopoietins), but Angptl1s do not bind to either Tie2 or the homologous Tie1 protein, indicating that their role differs from that of angiopoietins.

Here we show that angiopoietin-like protein 2 (Angptl2) is primarily secreted by adipose tissue and that its expression is increased by obesity and obesity-related pathological conditions, including hypoxia and endoplasmic reticulum (ER) stress. We found that increased circulating Angptl2 levels were closely related to adiposity, systemic insulin resistance, and inflammation in both mice and humans. Angptl2 acted on endothelial cells and monocytes/macrophages via integrin signaling, resulting in the promotion of inflammation. Constitutive activation of Angptl2 in mouse skin tissue induced chronic inflammation, including inflammatory changes of the vasculature characterized by abundant attachment of leukocytes to the vessel walls and increased

permeability. Deletion of Angptl2 led to reduced inflammation in adipose tissue and ameliorated systemic insulin resistance in mice with dietary obesity. Conversely, persistent overexpression of Angptl2 in adipose tissue caused local inflammation and systemic insulin resistance in nonobese mice. These findings establish Angptl2 as a key adipocyte-derived inflammatory mediator linking obesity to systemic insulin resistance and identify it as a new molecular target that could be used to improve the diagnosis and treatment of obesity and related metabolic diseases.

RESULTS

Angptl2 Expression in White Adipose Tissue Is Increased by Obesity and Obesity-Related Stress

Angptl2 mRNA was widely expressed in various organs of mice, but its level was particularly elevated in visceral white adipose tissues (Figure 1A). Differentiated 3T3-L1 adipocytes expressed Angptl2 mRNA (Figure 1B), and its expression was increased by hypoxia (Figure 1C), which occurs in obese adipose tissue (Hosogai et al., 2007; Nishimura et al., 2008; Schenk et al., 2008; Ye, 2009). We found significantly increased ER stress in adipocytes from obese mice compared with cells from nonobese mice (see Figure S1 available online). Serum levels of long-chain saturated fatty acids (LCSFAs) are elevated in obesity, and LCSFAs promote ER stress in adipocytes (Schenk et al., 2008). Our in vitro study of cultured 3T3-L1 cells revealed that ER stress was induced in adipocytes after treatment with palmitate, one of the LCSFA, or thapsigargin, an ER stress inducer. As

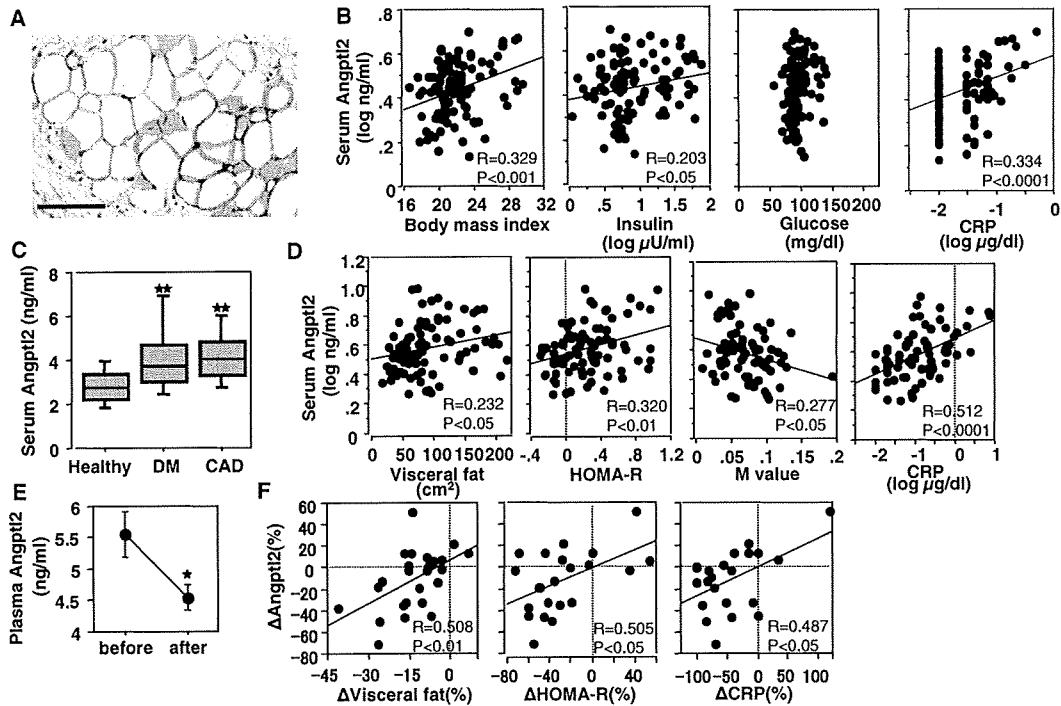


Figure 2. Circulating Angptl2 Is Correlated with Adiposity, Insulin Resistance, and Inflammation in Humans

(A) Immunohistochemical staining for Angptl2 in human adipose tissue. Scale bar, 100 μ m.
 (B) Correlation of the serum Angptl2 level with the body mass index or serum insulin, glucose, and CRP levels in healthy volunteers (n = 98).
 (C) Serum Angptl2 levels in healthy volunteers (Healthy, n = 98) and in patients with type 2 diabetes (DM, n = 89) or coronary artery disease (CAD, n = 109). Horizontal bars represent the 10%–90% percentile range, and boxes indicate the 25%–75% percentile range. The horizontal line in each box corresponds to the median.
 (D) Correlation of the serum Angptl2 level with the visceral fat area, HOMA-R index, M value, and CRP level in diabetic patients.
 (E and F) Changes of the plasma Angptl2 level in obese diabetic male patients after pioglitazone treatment (n = 27). Plasma Angptl2 levels (mean \pm SEM) before and after treatment (E). Correlation of the change (%) of the plasma Angptl2 level with the change (%) of the visceral fat area, subcutaneous fat area, HOMA-R index, and CRP level. Correlation coefficient (R) and probability (P) values are shown (F). *p < 0.05 and **p < 0.01 compared with controls.

a result, both the cellular Angptl2 mRNA level and its protein concentration in the culture medium were significantly increased (Figures 1D and 1E, Figure S2, and data not shown). Angptl2 mRNA in mesenteric white adipose tissue and serum Angptl2 protein levels were increased in obese mice fed a high-fat diet (Figures 1F and 1G), suggesting that Angptl2 is a bioactive adipocyte-derived factor that has a role in obesity and related metabolic diseases.

Circulating Angptl2 Level Is Correlated with Adiposity, Systemic Insulin Resistance, and Inflammation in Humans

Immunohistochemical analysis revealed that Angptl2 was expressed by the adipocytes of human adipose tissue (Figure 2A). We analyzed the circulating levels of Angptl2 in various human subjects by using an enzyme-linked immunosorbent assay (ELISA). In healthy normal-weight volunteers aged from 20 to 59 years, the serum Angptl2 concentration ranged from 1.36 to 4.98 ng/ml, and the distribution was normal after log transformation (Figure S3A). Plasma levels were comparable and strongly correlated with the corresponding serum levels (Figure S3B). There was no significant difference of serum Angptl2 concentra-

tion between genders (data not shown). Angptl2 level showed a positive correlation with body mass index, serum insulin level, and serum C-reactive protein (CRP) level. In contrast, the level of Angptl4, which has already been identified as an adipocyte-derived Angptl, showed no correlation with these factors in normal-weight healthy subjects (Figure 2B and Figure S4). An increase of the body mass index, serum insulin level, and CRP level is associated with the development of type 2 diabetes and atherosclerosis (Eckel et al., 2005; Mokdad et al., 2003). Indeed, serum Angptl2 was also significantly increased in patients with type 2 diabetes or coronary artery disease (Figure 2C). In 935 consecutive persons aged 27–84 years who underwent a medical checkup and gave informed consent for measurement of serum Angptl2 at the Japanese Red Cross Kumamoto Health Care Center, the Angptl2 level was positively correlated with the body mass index, abdominal circumference, and serum CRP level (Figure S5). In patients with type 2 diabetes, Angptl2 was positively correlated with the visceral fat area, homeostasis model assessment of insulin resistance (HOMA-R) index (Matthews et al., 1985), and serum CRP level, but not with the subcutaneous fat area. Angptl2 level was inversely correlated with the insulin sensitivity index (M value), as assessed

by the hyperinsulinemic euglycemic clamp test (DeFronzo et al., 1979) (Figure 2D).

These observations led us to ask whether improvement of systemic insulin resistance or inflammation would influence the circulating level of Angptl2. We observed a significant decrease of the plasma Angptl2 level in 27 obese diabetic men following treatment with pioglitazone at 30 mg/day for 3 months (Figure 2E). The percent decrease of the plasma Angptl2 level was correlated with the percent decrease of the visceral fat area, HOMA-R index, and serum CRP level (Figure 2F). These results suggested that visceral fat was likely to be the main source of circulating Angptl2, the concentration of which was significantly correlated with systemic insulin resistance and inflammation.

Angptl2 Activates Migration and Inflammatory Changes of Endothelial Cells and Monocytes/Macrophages via Integrins

Since the vasculature has an important role in tissue inflammation (Jackson et al., 1997), we examined the effect of Angptl2 on endothelial cells. First, we found a dose-dependent increase of cell adhesion when human umbilical vein endothelial cells (HUVECs) and human arterial endothelial cells (HAECs), which express several integrins on their surfaces, were plated on Angptl2-coated plates (Figures 3A and S6). We next analyzed cell adhesion in the presence of a series of function-blocking antibodies for specific integrins. A neutralizing antibody for integrin $\alpha 5\beta 1$ inhibited endothelial cell adhesion to Angptl2-coated plates, as did RGD peptide, which blocks RGD-dependent integrins (Figure 3B), suggesting that Angptl2-induced endothelial cell adhesion was an $\alpha 5\beta 1$ -dependent process, although the involvement of untested integrins could not be excluded. Integrin $\alpha 5\beta 1$ activates NF- κ B in endothelial cells (Klein et al., 2002). Consistently, there was increased translocation of NF- κ B to the nucleus and degradation of I κ B in HUVECs stimulated with recombinant human Angptl2 protein (Figures 3C and 3D).

Angptl2 also promoted the migration of HUVECs and HAECs through a microchemotaxis membrane (Figure 3E). Time-lapse imaging of HUVECs or HAECs cultures revealed that protrusion of lamellipodia and membrane ruffling were rapidly induced following the addition of Angptl2 (Movies S1 and S2). Since Rac1, a small Rho-GTPase, plays a pivotal role in the protrusion of lamellipodia, membrane ruffling, and cell migration (Bar-Sagi and Hall, 2000; Fryer and Field, 2005), we investigated whether Rac1 was activated in HAECs and HUVECs by performing a pull-down assay. Activation of Rac1 was detected in both Angptl2-stimulated HUVECs and HAECs (Figure 3F). In viable Angptl2-stimulated HUVECs, a single-molecule probe was used to determine Rac1 activity, showing that it was diffusely activated at the plasma membrane, with this activation being followed by protrusion of lamellipodia and membrane ruffling (Figure 3G and Movie S3). Moreover, Angptl2 no longer stimulated the protrusion of lamellipodia and membrane ruffling in HUVECs transfected with a dominant-negative Rac1 mutant expressing red fluorescent protein (RacN17-IRES-RFP) (Figure 3H and Movie S4). These findings suggest that Angptl2-stimulated lamellipodia formation and membrane ruffling in endothelial cells were both mediated by activation of Rac1. Next, we investigated whether Angptl2 could induce in vivo chemotaxis

of endothelial cells in a mouse cornea assay. Implanted pellets containing Angptl2 markedly induced neovascularization in the mouse cornea, whereas pellets containing PBS alone did not (Figure 3I). Monocytes/macrophages express several integrin receptors that are responsible for adhesion, migration, and extravasation into the peripheral tissues (Friedl and Weigelin, 2008; Rose et al., 2007). We found that the THP-1 human monocytic cell line expressed integrins $\alpha 4$, $\beta 1$, $\beta 2$, and $\alpha 5\beta 1$ (Figure 3J). THP-1 cells adhered to Angptl2-coated plates in a dose-dependent manner (Figure 3K). FACS analysis revealed that Angptl2 bound to THP-1; this binding was completely inhibited by neutralizing antibodies for integrins $\alpha 4$ or $\beta 2$ and was partially blocked by antibodies for integrin $\alpha 5\beta 1$ or $\beta 1$ (Figure 3L). Angptl2 also promoted transmigration by THP-1 cells and primary human monocytes (Figure 3M and Figure S7).

Constitutive Angptl2 Activation Induces Local Inflammation in Mouse Skin Tissue

To further investigate the role of Angptl2 in the inflammatory process, we generated transgenic mice expressing Angptl2 driven by the keratinocyte-specific promoter K14 (K14-Angptl2) and therefore constitutively expressing Angptl2 in the epidermis (Figures S8A and S8B). The ears, snouts, and eyelids of K14-Angptl2 mice were redder than those of controls. The tails of K14-Angptl2 mice were not only reddish but also swollen and showed loss at the tips (Figure 4A), indicating local inflammation. Lectin staining showed an increase of adherent leukocytes, a common feature of inflammatory vasculature (McDonald, 1994), in enlarged vessels of the skin tissue specimens from K14-Angptl2 mice (Figure 4B), while there was no difference of vessel length between the genotypes (Figure S8C). The vessels of K14-Angptl2 mice were significantly more permeable than the vessels of wild-type controls after inflammation was induced by topical application of mustard oil, a potent proinflammatory agent (Figure 4C). As expected, even before mustard oil application, lumens of CD31⁺LYVE-1⁺ lymphatics were enlarged in the skin of K14-Angptl2 mice, while such changes were not observed in controls (Figure 4D), suggesting that increased drainage via lymphatics was compensating for the excessive leakiness of Angptl2-stimulated vessels in the dermis. These findings indicate that Angptl2 induces inflammatory vascular remodeling rather than angiogenesis.

Reduction of Adiposity and Obesity-Related Adipose Tissue Inflammation in *Angptl2*^{-/-} Mice

Next, we investigated the pathophysiological role of Angptl2 by generating Angptl2 knockout (*Angptl2*^{-/-}) mice (Figure S9). *Angptl2*^{-/-} mice were born alive following Mendelian inheritance and appeared to be grossly normal. Interestingly, when fed normal chow, *Angptl2*^{-/-} mice weighed slightly less (Figure S10A) and had a lower body fat mass estimated by computed tomography (CT) (Figures S10B and S10C) than heterozygotes or wild-type mice fed the same normal diet, although there was no significant difference of daily food intake or energy expenditure between the groups (Figures S10D and S10E). In addition, *Angptl2*^{-/-} mice showed slightly, but significant, better glucose tolerance and insulin sensitivity (Figures S10F and S10G). Next, we fed 8-week-old mice a high-fat diet containing 32% (wt/wt) fat to stimulate weight gain. After

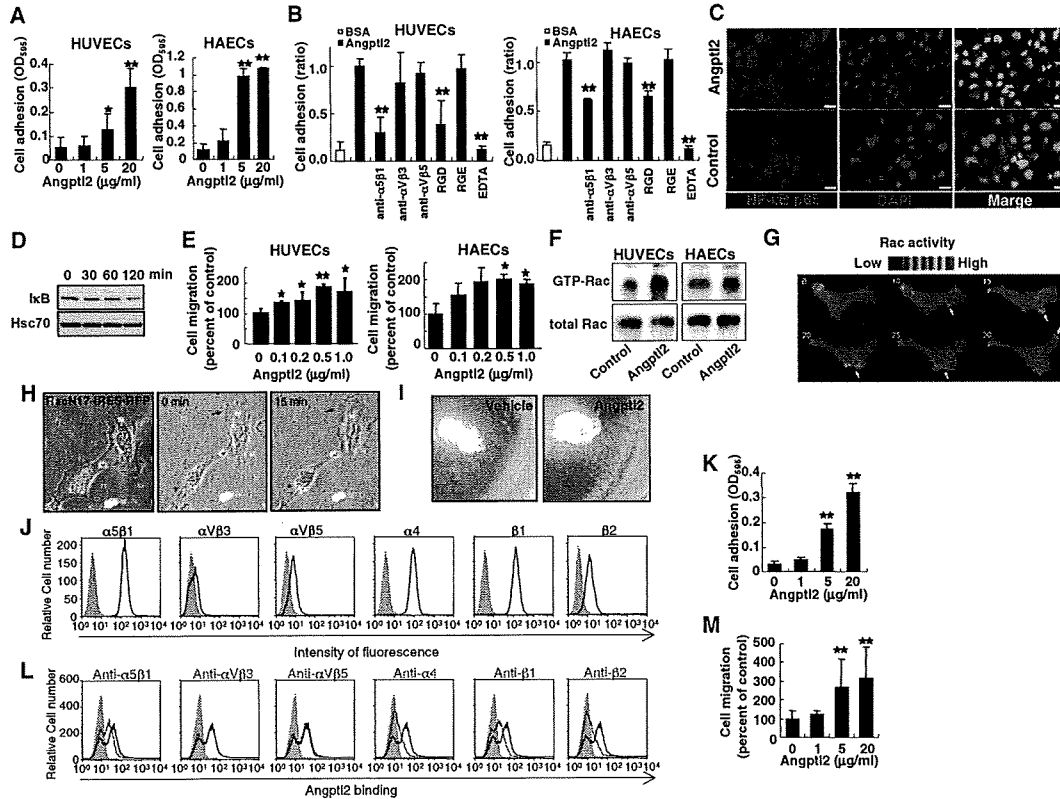


Figure 3. Angptl2 Activates Endothelial Cells and Monocytes

(A) Adhesion of HUVECs or HAECs to culture dishes coated with various concentrations of recombinant human Angptl2 ($n = 3$). (B) HUVECs or HAECs were preincubated with or without 25 $\mu\text{g/ml}$ of blocking antibodies (anti- $\alpha 5\beta 1$, anti- $\alpha v\beta 3$, or anti- $\alpha v\beta 5$) or RGD or RGE peptides (300 μM), and cell adhesion was assessed ($n = 3$). As a negative control, cell adhesion was assayed in the presence of 10 μM EDTA, which inhibits integrin binding. (C) Nuclear translocation of NF- κ B subunit p65 in HUVECs at 2 hr after Angptl2 stimulation. Nuclei were counterstained with 4',6'-diamidino-2-phenylindole (DAPI). Scale bar, 20 μm . (D) Representative western blots of I κ B and Hsc70 protein (internal control) in HUVECs at the indicated times after Angptl2 stimulation. (E) Migration of HUVECs or HAECs in response to Angptl2 ($n = 4$). (F) HUVECs or HAECs were cultured with Angptl2 for 30 min and then subjected to the pull-down assay using GST-PAK-CRIB followed by western blotting with anti-Rac1 antibody. Representative images are shown. (G) HUVECs expressing Raichu-Rac1 (a probe for active Rac1) at the indicated times (min) after Angptl2 stimulation. Arrows indicate nascent and retracting lamellipodia. Ratio ranges are shown on the right. (H) HUVECs that were either untransfected or transfected with RacN17 (shown in red in the left panel and by red stars in the center and right panels) and stimulated with Angptl2 at time 0 and 15 min. Angptl2-stimulated membrane ruffling is observed in HUVECs without RacN17 (arrows). (I) Macroscopic appearance of neovascularization in the mouse cornea. Pellets containing vehicle or Angptl2 (0.5 μg) were implanted into micropockets cut in the corneal stroma. (J) Integrin expression by THP-1 cells. Typical profiles obtained by FACS analysis with the indicated anti-integrin antibodies (black line traces) or isotype-matched control IgG (filled gray traces). (K) Adhesion of THP-1 cells to culture dishes coated with various concentrations of Angptl2 ($n = 3$). (L) Inhibition of Angptl2 binding to THP-1 cells by integrin-neutralizing antibodies. THP-1 cells were preincubated with (red line traces) or without (blue line traces) the indicated anti-integrin neutralizing antibodies, and then incubated with FLAG-tagged Angptl2 followed by detection with FITC-conjugated anti-FLAG antibody. Negative controls (filled gray traces) had omission of Angptl2. (M) Migration of THP-1 cells in response to Angptl2 ($n = 7-9$). Data are the mean \pm SD, * $p < 0.05$ and ** $p < 0.01$ compared with controls.

8 weeks of high-fat diet feeding, *Angptl2*^{-/-} mice had a body weight 12% lower than that of wild-type mice (Figure 5A). The visceral and subcutaneous fat mass and total body fat percentage were moderately decreased in *Angptl2*^{-/-} mice compared to wild-type mice (Figures 5B and 5C). Considerable accumulation of fat was seen in the liver and skeletal muscle of wild-type mice, whereas these changes were mild in *Angptl2*^{-/-}

mice (Figures 5D and 5E). Although there were no obvious differences of food intake or energy expenditure between the two groups, the respiratory quotient was significantly lower in the *Angptl2*^{-/-} group (Figures S11A-S11C).

We next examined the expression of mRNAs for inflammatory cytokines (IL-6 and TNF- α), a chemokine (MCP-1), various macrophage markers (F4/80, CD68, CCR2, Mgl1, and Mgl2),

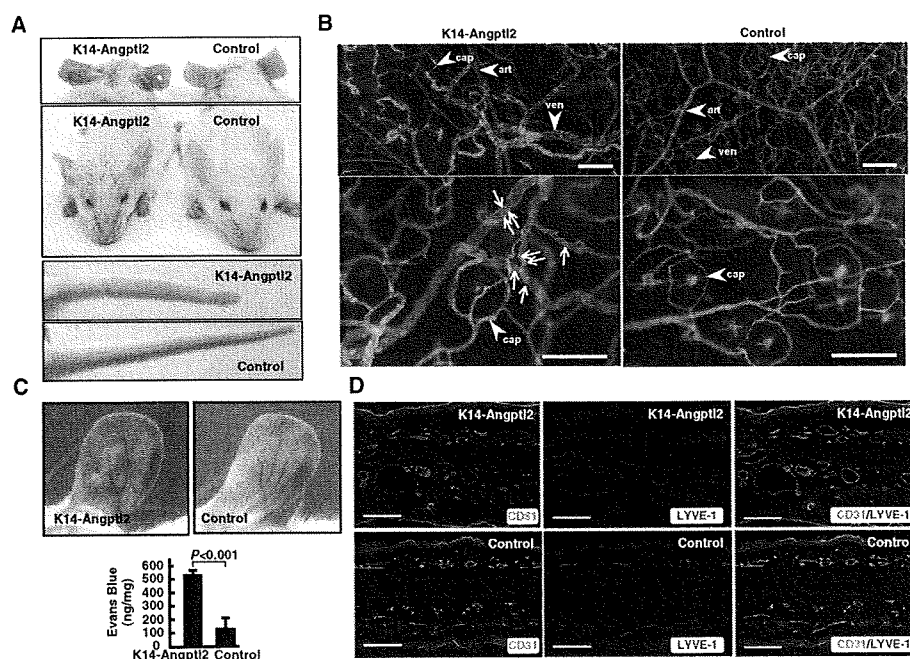


Figure 4. Sustained Angptl2 Overexpression Induces Vascular Inflammation

(A) Appearance of 6-month-old transgenic K14-Angptl2 and control mice.
 (B) Ear skin blood vessels from transgenic and control mice. Arrows indicate adherent leukocytes on the walls of enlarged vessels from K14-Angptl2 mice. Arrowheads with art, ven, and cap in each panel indicate arteriole, venule, and capillary, respectively. Scale bar, 200 μ m.
 (C) Evans blue dye leakage into the skin of the ear following treatment with mustard oil as an inflammatory agent. Representative images and quantitative values are shown (mean \pm SD, n = 7).
 (D) Immunohistochemistry of ear skin from K14-Angptl2 and control mice with anti-CD31 and anti-LYVE-1 antibodies. Representative photographs are shown. Scale bar, 100 μ m.

and insulin-sensitizing adipocytokines (adiponectin and leptin) in the adipose tissue of mice fed a high-fat diet. As shown in Figure 5F, adiponectin expression was increased, while TNF- α and general (F4/80, CD68) and inflammatory (CCR2) macrophage markers were all decreased in the adipose tissue of *Angptl2*^{-/-} mice. However, the expression of residential macrophage markers (Mgl1 and Mgl2) remained unchanged. Furthermore, expression of F4/80 mRNA was positively correlated with the adipose tissue weight in controls, indicating that adiposity was significantly correlated with macrophage infiltration into adipose tissue. In contrast, there was no significant correlation between adipose tissue weight and macrophage infiltration in *Angptl2*^{-/-} mice (Figure 5G), suggesting that this decrease of macrophage infiltration may be independent of reduced adiposity in *Angptl2*^{-/-} mice. Furthermore, immunohistochemistry using the macrophage marker Mac2 revealed accumulation of Mac2-positive macrophages in crown-like structures within the adipose tissue of wild-type mice, while fewer Mac2-positive cells were observed in the adipose tissue of *Angptl2*^{-/-} mice (Figure 5H). The high-fat diet caused impaired glucose tolerance and insulin resistance in controls, whereas *Angptl2*^{-/-} mice showed better glucose tolerance and insulin sensitivity based on the results of intraperitoneal glucose and insulin tolerance tests (GTT and ITT, respectively) (Figures 5I and 5J). To explore which organ(s) contributed to the improved insulin sensitivity in *Angptl2*^{-/-} mice, we next performed western blotting

analysis of the insulin signaling pathway. Tyrosine phosphorylation of insulin receptor β and serine phosphorylation of Akt after insulin injection were significantly increased in both the liver and skeletal muscle of *Angptl2*^{-/-} mice compared with wild-type mice (Figure 5K). To confirm these results, we performed hyperinsulinemic-euglycemic clamp experiments. Both glucose infusion rate and whole-body glucose disposal rate were significantly increased in *Angptl2*^{-/-} mice, while clamp endogenous glucose production was significantly reduced. In addition, the percent decrease in endogenous glucose production from basal to clamp states was significantly higher in *Angptl2*^{-/-} mice than in wild-type mice (Figure 5L). These results indicated that insulin sensitivity was improved in both the skeletal muscle and liver of *Angptl2*^{-/-} mice fed a high-fat diet.

Angptl2 Promotes Local Inflammation in Adipose Tissue and Systemic Insulin Resistance

Finally, we determined whether sustained overexpression of Angptl2 in adipose tissue promoted systemic insulin resistance by generating transgenic mice that overexpressed Angptl2 in adipose tissue under the control of aP2, an adipose tissue-specific promoter (aP2-Angptl2) (Figure S12A). Based on the level of Angptl2 expression, we considered that line 5 was the most acceptable model for examining the pathological role of increased Angptl2 expression in obese mice (Figure S12B), so we performed subsequent analyses using line 5 and wild-type

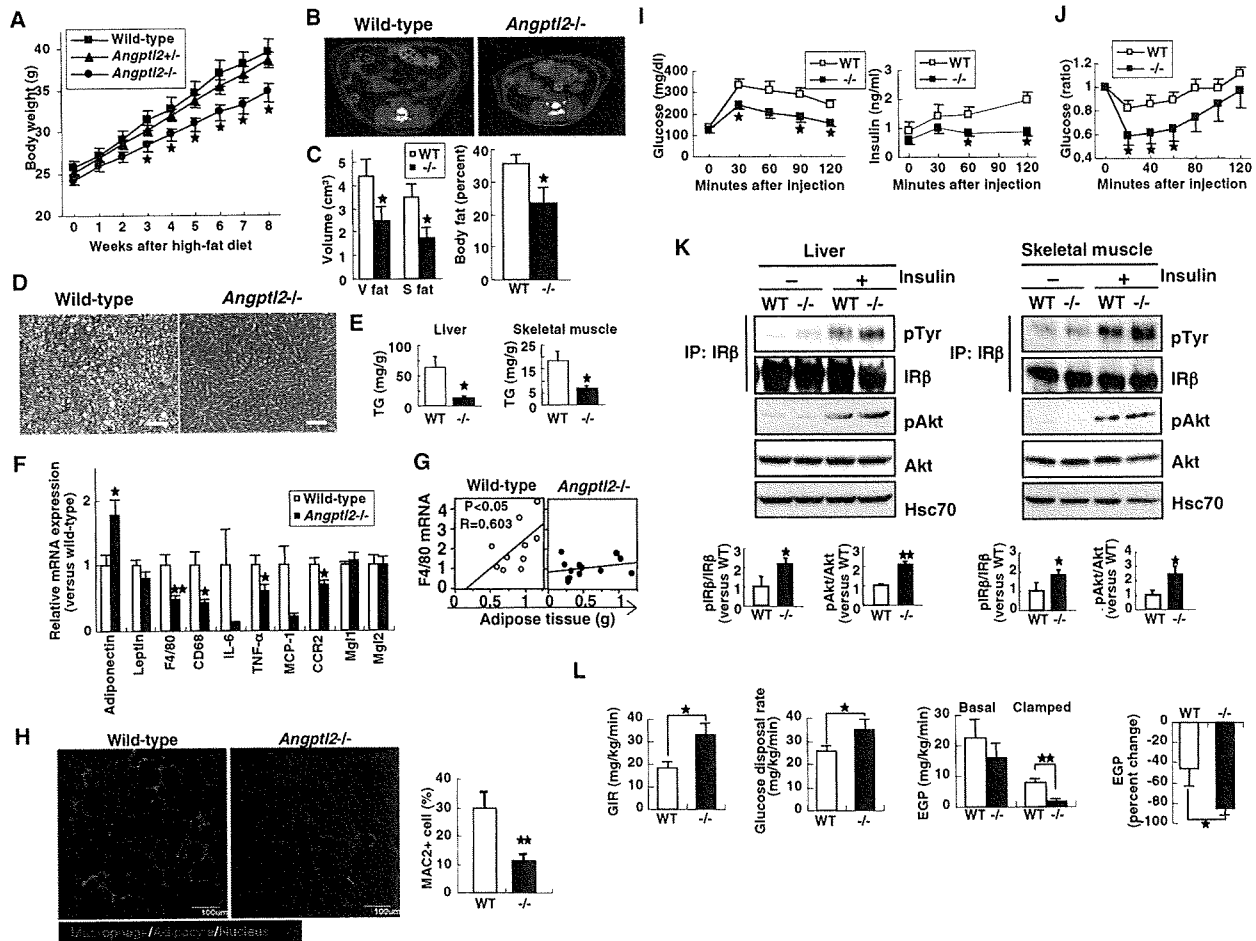


Figure 5. Deletion of *Angptl2* Reduces Adipose Tissue Inflammation and Systemic Insulin Resistance in Dietary Obese Mice

Analyses of *Angptl2*^{-/-} and wild-type mice fed a HFD for 8 weeks (A–L).

(A) Body weight of each genotype (n = 8–16 per group) at the indicated times (weeks) after initiation of a HFD.

(B and C) Representative CT findings (B) and quantitative comparison of the visceral (V) and subcutaneous (S) fat volume and total percent body fat (C) in *Angptl2*^{-/-} mice and wild-type mice (n = 5–7 per group).

(D) HE-stained liver sections from *Angptl2*^{-/-} and wild-type mice. Scale bar, 100 μ m.

(E) Triglyceride (TG) content of liver and skeletal muscle from *Angptl2*^{-/-} mice and wild-type mice (n = 6 per group).

(F) Quantitative RT-PCR of mRNAs encoding adipocytokines and macrophage markers in epididymal adipose tissue from *Angptl2*^{-/-} and wild-type mice (n = 11–12 per group).

(G) Correlation between F4/80 mRNA expression and epididymal adipose tissue weight in *Angptl2*^{-/-} mice and wild-type mice (n = 11–12 per group). Correlation coefficient (R) and probability (P) values are shown.

(H) Immunohistochemistry of adipose tissue using the macrophage marker MAC2 and adipocyte marker perillipin. Representative photographs and quantitative comparisons of MAC2-positive cells (n = 6 per group) are shown. Scale bar, 100 μ m.

(I and J) Glucose (I) and insulin (J) tolerance tests in *Angptl2*^{-/-} mice and wild-type mice (n = 5 and n = 10 per group, respectively).

(K) Insulin signaling in the liver and skeletal muscle of *Angptl2*^{-/-} (KO) and wild-type (WT) mice. Representative western blots and quantitative data for the total and phosphorylated forms of insulin receptor β subunit (IR β) and Akt are shown (n = 4 per group).

(L) Glucose infusion rate (GIR), glucose disposal rate, endogenous glucose production (EGP) during the basal and clamped states, and percent change in EGP between the states in *Angptl2*^{-/-} (KO) and wild-type (WT) mice (n = 5–7 per group). Data are mean \pm SEM, *p < 0.05 and **p < 0.01 compared with controls.

littermates as controls. There was no difference of weight gain between aP2-Angptl2 mice and control wild-type mice fed a normal chow diet (Figure 6A). However, immunohistochemistry using Mac2 revealed accumulation of macrophages in crown-like structures within the adipose tissue of aP2-Angptl2 mice, whereas fewer Mac2-positive cells were observed in wild-type mice (Figure 6B). RT-PCR analysis revealed that inflammatory

cytokines (IL-6, TNF- α , and IL-1 β) and general (CD68) and inflammatory (CCR2) macrophage markers were increased in the adipose tissue of aP2-Angptl2 mice, while adiponectin and leptin were unchanged (Figure 6C). Lectin staining showed an increase of adherent leukocytes in vessels within the adipose tissue of aP2-Angptl2 mice, while few leukocytes were detected in the vessels of wild-type mice (Figure 6D). There was no

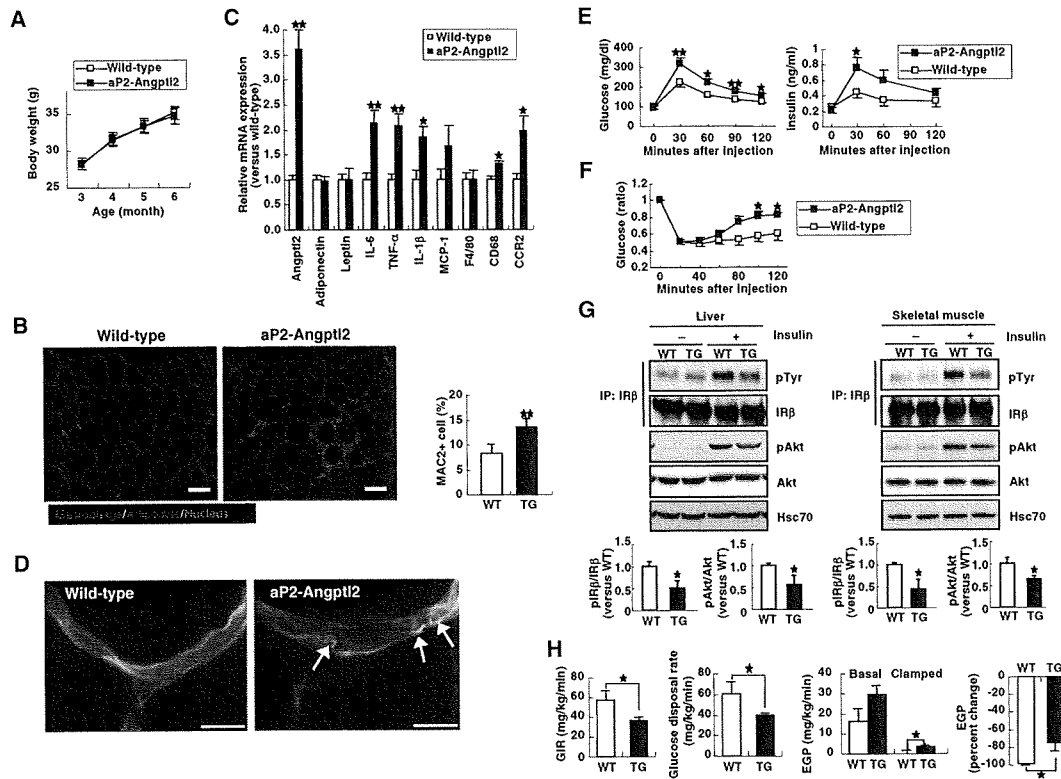


Figure 6. Angptl2 in Adipose Tissue Induces Local Inflammation and Systemic Insulin Resistance

Analyses of aP2-Angptl2 and wild-type mice at 16 weeks of age (B–H).

(A) Body weight of aP2-Angptl2 and wild-type mice ($n = 14\text{--}16$ per group) at the indicated ages (months).

(B) Immunohistochemistry of adipose tissue using the macrophage marker MAC2 and adipocyte marker perillipin. Representative photographs and quantitative comparison of MAC2-positive cells are shown ($n = 6$ per group). Scale bar, 50 μm .

(C) Quantitative RT-PCR of mRNAs encoding adipocytokines and macrophage markers in epididymal adipose tissue from aP2-Angptl2 mice and wild-type mice ($n = 6$ per group).

(D) Blood vessels in epididymal adipose tissue from aP2-Angptl2 and wild-type mice. Arrows indicate adherent leukocytes on the walls of enlarged vessels in aP2-Angptl2 mice. Scale bar, 25 μm .

(E and F) Glucose (E) and insulin (F) tolerance tests in aP2-Angptl2 mice and wild-type mice ($n = 10\text{--}12$ per group).

(G) Insulin signaling in the liver and skeletal muscle of aP2-Angptl2 (TG) and wild-type (WT) mice. Representative western blots and quantitative data for the total and phosphorylated forms of insulin receptor β subunit (IR β) and Akt are shown ($n = 4$ per group).

(H) Glucose infusion rate (GIR), glucose disposal rate, endogenous glucose production (EGP) during the basal and clamped states, and percent change in EGP between the states in aP2-Angptl2 (TG) and wild-type (WT) mice ($n = 7$ per group). Data are mean \pm SEM, * $p < 0.05$ and ** $p < 0.01$ compared with controls.

difference of blood vessel density between aP2-Angptl2 mice and control mice (Figure S12C). aP2-Angptl2 showed glucose intolerance and insulin resistance in the GTT and ITT, respectively (Figures 6E and 6F). Insulin signaling was diminished in both liver and skeletal muscle of aP2-Angptl2 mice compared with wild-type mice (Figure 6G). The hyperinsulinemic-euglycemic clamp tests also revealed insulin resistance in both skeletal muscle and liver of aP2-Angptl2 mice, since the glucose infusion rate, whole-body glucose disposal rate, and percent change of endogenous glucose production between basal and clamp states were reduced in aP2-Angptl2 mice compared with wild-type mice, while hepatic glucose production during the clamp period was increased in aP2-Angptl2 mice compared with control mice (Figure 6H). These results indicated the presence of insulin resistance in both the skeletal muscle and liver of nonobese aP2-Angptl2 mice.

DISCUSSION

We demonstrated that Angptl2, a member of the Angptl family, is a key mediator of chronic adipose tissue inflammation and obesity-related systemic insulin resistance.

Here we showed that Angptl2 is an adipocyte-derived inflammatory mediator, with increased expression at both the mRNA and protein levels in obesity. Hypoxia and ER stress, which are enhanced in obese adipose tissue (Hosogai et al., 2007; Nishimura et al., 2008; Schenk et al., 2008; Ye, 2009), both increased Angptl2 expression or secretion in adipocytes. Various changes of the microenvironment observed in the adipose tissue of obese animals, such as inflammation and hypoxia, could also promote ER stress (Schenk et al., 2008). Therefore, Angptl2 production by adipocyte should be increased by hypoxia and ER stress in obesity.

It is noteworthy that the circulating Angptl2 level was positively correlated with obesity-related metabolic changes. The difference of circulating Angptl2 protein levels between Angptl2 Tg mice and wild-type mice was only 1.5-fold, but tissue Angptl2 levels showed a 3- to 5-fold difference (data not shown). Therefore, the modest difference of circulating Angptl2 levels in humans may reflect a larger alteration of adipose tissue Angptl2 expression, which could promote inflammation of adipose tissue, resulting in systemic insulin resistance. We also do not exclude the possibility that there is a direct inhibitory effect of circulating Angptl2 on insulin sensitivity in other peripheral tissues, such as skeletal muscle or the liver, because glucose clamp studies and western blotting analysis of insulin signaling revealed that both skeletal muscle and liver were target organs for Angptl2-related insulin resistance in mice. Other Angptl family molecules function in an endocrine manner to regulate lipids, glucose, and energy metabolism (Hato et al., 2008; Oike et al., 2005a, 2005b), so further studies are needed to clarify whether Angptl2 might also act in an endocrine manner.

Angptl2 contains an N-terminal coiled-coil domain and a C-terminal fibrinogen-like domain. The coiled-coil domain is required for oligomerization, which is necessary for its maximum activity, while the fibrinogen-like domain shares high homology with the analogous domain of fibrinogen. Fibrinogen acts as a ligand of the receptors for integrins such as $\alpha v\beta 3$, $\alpha 5\beta 1$, and $\alpha M\beta 2$ (Herrick et al., 1999; Mosesson, 2005), which are heterodimeric transmembrane glycoproteins that mediate cell-extracellular matrix and cell-cell adhesion (Hynes, 2002). Angptl3 was reported to promote angiogenesis through integrin $\alpha v\beta 3$ (Camenisch et al., 2002). In this study, we found that Angptl2 acted on endothelial cells through integrin $\alpha 5\beta 1$ and influenced monocytes/macrophages through integrins $\alpha 4$ or $\beta 2$. Several reports have indicated that integrin $\alpha 5\beta 1$ signaling activates Rac1 in endothelial cells (Dormond et al., 2001; Mettouchi et al., 2001), in agreement with our finding that Angptl2 promotes Rac1 activation in endothelial cells. We also found that Angptl2 induced the chemotaxis of endothelial cells by *in vitro* time-lapse imaging analysis and an *in vivo* mouse cornea neovascularization assay. In contrast, constitutive overexpression of Angptl2 in mouse skin or adipose tissue induced pathological vascular inflammation but did not increase vascularization or ameliorate hypoxia in the adipose tissue of mice with dietary obesity (Figure S12D). The cornea is an avascular tissue and thus is isolated from circulating soluble bioactive mediators, whereas various angiogenesis-related factors exist in highly vascular tissues such as the skin and adipose tissue. Taken together, these findings indicate that Angptl2 may function differently in different tissues, but it promotes vascular inflammation rather than angiogenesis, at least in adipose tissue that develops in obese mice.

Potentially relevant to these findings, we observed that Angptl2 stimulated the nuclear translocation of NF- κ B and degradation of I κ B in cultured vascular endothelial cells, findings consistent with a previous report that integrin $\alpha 5\beta 1$ signaling activates NF- κ B-dependent expression of genes that are important for inflammation (Klein et al., 2002). There have been several other reports that Rac1 activates NF- κ B (Perona et al., 1997; Sulciner et al., 1996), which is also consistent with our findings. An important aspect of inflammation is the recruitment of immune cells to affected tissues (Luster et al., 2005). This

process requires adhesion of the immune cells to endothelial cells, allowing extravasation into the interstitium, followed by adhesion of immune cells to the extracellular matrix that enables migration toward the site of inflammation. In this regard, Angptl2 not only activated NF- κ B in endothelial cells, which could induce expression of adhesion molecules (such as ICAM, VCAM, and selectin) and thus facilitate adhesion of immune cells to endothelial cells, but also promoted the migration of monocytes. Immune cells express integrins $\alpha 4$ or $\beta 2$, as well as $\alpha 5\beta 1$, which mediate cell adhesion, migration, activation, and production of proinflammatory cytokines through activation of NF- κ B (Hynes, 2002; Rose et al., 2007; Roman et al., 2004; Graves and Roman, 1996), suggesting that Angptl2 may activate monocytes via such integrins. It remains to be clarified whether only Angptl2 among the Angptl family shows a stimulatory effect on adipose tissue inflammation, because some other members of this family bind to integrins (Camenisch et al., 2002), and Angptl4 is also abundantly expressed in adipose tissue. The skin tissue of K14-Angptl4 mice showed no inflammatory changes (Ito et al., 2003), unlike that of K14-Angptl2 mice. Moreover, there was no correlation between the serum Angptl4 concentration and Angptl2-related metabolic factors. These findings suggest that the effects of Angptl4 on endothelial cells and/or immune cells are different from those of Angptl2.

In this study, we demonstrated that Angptl2 deletion not only ameliorated inflammation in adipose tissue but also improved systemic insulin resistance in mice with dietary obesity, although it did not completely normalize their insulin sensitivity to the level seen in mice fed a normal chow diet (Figure S11I). The restoration of insulin sensitivity related to Angptl2 deletion may be attributable to the difference of body fat accumulation between the two genotypes. Since adipose tissue volume was not correlated with macrophage infiltration in *Angptl2*^{-/-} mice, some mechanism other than the difference of adiposity may also have contributed to reducing adipose tissue inflammation in *Angptl2*^{-/-} mice. Actually, constitutive Angptl2 overexpression in adipose tissue induced both local inflammation and systemic insulin resistance in nonobese mice. Since adipose tissue inflammation can be a cause of systemic insulin resistance via the secretion of several inflammatory factors (Apovian et al., 2008; Neels and Olefsky, 2006; Schenk et al., 2008), it is suggested that Angptl2 probably influenced systemic insulin sensitivity by exacerbating adipose tissue inflammation (Figure S13).

Although a reduction of adipose tissue inflammation could well be the main reason for improvement of insulin sensitivity in *Angptl2*^{-/-} mice, some other possible mechanisms remain. Adiponectin can potentially increase insulin sensitivity, and the adiponectin level is usually decreased in obesity (Kadowaki and Yamauchi, 2005). However, there was no difference of circulating adiponectin levels between *Angptl2*^{-/-} and control mice (Figure S11H). On the other hand, *Angptl2*^{-/-} mice had a reduced triglyceride content in both skeletal muscle and liver, which could improve insulin sensitivity in these two organs (Schenk et al., 2008).

Angptl2^{-/-} mice showed reduced body fat and tissue triglyceride accumulation when fed a high-fat diet, although there was no obvious difference of daily food intake and energy expenditure estimated from the O₂ consumption rate. Interestingly, the respiratory quotient of *Angptl2*^{-/-} mice was significantly lower

than that of wild-type mice, suggesting that *Angptl2*^{-/-} mice were more likely to use lipids than carbohydrates for oxidation to create energy. There was also a trend of increased expression of lipid oxidation genes in the skeletal muscle of *Angptl2*^{-/-} mice and increased UCP1 expression in brown adipose tissue (Figures S11D and S11F), which may account for the lower respiratory quotient, decreased triglyceride content of skeletal muscle, and decrease of whole-body fat in *Angptl2*^{-/-} mice. On the other hand, the hepatic expression of lipogenic genes (SREBP-1c, FAS, and SCD1) was significantly decreased in *Angptl2*^{-/-} mice (Figure S11G), which explains the decreased triglyceride content in the liver of these mice, although further studies will be needed to clarify the molecular mechanisms involved.

In summary, this study provided evidence that Angptl2 plays a key role in inflammation of adipose tissue via inflammatory vascular remodeling and recruitment of macrophages into adipose tissue. These findings suggest that Angptl2 may be an important part of the mechanism underlying adipose tissue inflammation that is involved in the pathogenesis of systemic insulin resistance related to obesity. The present findings should also lead to new treatment strategies for obesity and related insulin resistance.

EXPERIMENTAL PROCEDURES

Materials and additional methods are available in the Supplemental Experimental Procedures.

Animal Study

All experimental protocols were approved by the Ethics Review Committee for Animal Experimentation of Kumamoto University. Only male mice were used for the experiments. For the metabolic analyses, mice at 8 weeks of age were fed either a normal diet (CE-2; CLEA, Japan) or a high-fat diet (HFD-32; CLEA) for a period of 8 weeks. During the analyses, mice continued to feed on the same diet.

Human Studies

White adipose tissue samples were obtained from the intact adipose tissue surrounding the tumor resected from a patient with pancreatic carcinoma. Samples were fixed in 4% paraformaldehyde for 24 hr and embedded in paraffin. Sections 5 μ m thick were cut and stained with an anti-Angptl2 polyclonal antibody (#383). Nuclei were counterstained with hematoxylin. A total of 98 volunteers working at Kumamoto University were enrolled in the study as the healthy group (persons with obesity [body mass index > 30] or diabetes were excluded). Blood samples were collected, and the plasma glucose, insulin, and CRP levels were measured. A total of 89 patients with type 2 diabetes were enrolled as the DM group. Their abdominal fat content was evaluated by magnetic resonance imaging. The HOMA-R index was calculated as the product of fasting plasma insulin (μ U/ml) and fasting plasma glucose (mg/dl) divided by 405 (Matthews et al., 1985). The euglycemic-hyperinsulinemic clamp test was carried out according to a protocol described elsewhere (DeFronzo et al., 1979). A total of 109 patients with coronary artery disease (diagnosed by coronary angiography) were enrolled as the CAD group, and blood samples were collected. Twenty-seven obese diabetic men who had not previously received any antidiabetic agents, antihypertensive agents, or lipid-lowering drugs were treated with pioglitazone at a dose of 30 mg/day for 3 months. Before and after treatment, the abdominal fat content was evaluated by CT scanning, and fasting blood samples were collected to measure the levels of glucose, insulin, and CRP. Blood samples were also collected from 935 consecutive volunteers aged 27–84 years, who underwent medical checkups at the Japanese Red Cross Kumamoto Health Care Center. Serum or plasma levels of Angptl2 and Angptl4 were measured by ELISA. This study was approved by the Ethics Committees of Kumamoto University (healthy and

CAD groups), Kobe University (DM group), Ryukyu University (pioglitazone study), and the Japanese Red Cross Kumamoto Health Care Center. Written informed consent was obtained from each subject.

SUPPLEMENTAL DATA

Supplemental Data include Supplemental Experimental Procedures, Supplemental References, 13 figures, one table, and four movies and can be found with this article online at [http://www.cell.com/cell-metabolism/supplemental/S1550-4131\(09\)00232-0](http://www.cell.com/cell-metabolism/supplemental/S1550-4131(09)00232-0).

ACKNOWLEDGMENTS

We would like to thank Ms. K. Fukushima, I. Ishimatsu, R. Shindo, Y. Indo, S. Iwaki, and O. Takahashi for experimental assistance; and Drs. S. Fuchigami, K. Yasunaga, N. Yamaji, and A. Sakurai for experimental assistance and helpful discussion. This work was supported by Grants-in-Aid for Scientific Research on Priority Areas (17014078) from the Ministry of Education, Culture, Sports, Science and Technology of Japan; by Grants-in Aid for Scientific Research (B) (21390245) from Japan Society for Promotion of Science; by a grant from the Mochida Memorial Foundation; by a grant from the Takeda Science Foundation; by a grant from the Sumitomo Foundation; by a grant from the Uehara Memorial Foundation; and by a grant from the Cell Science Research Foundation.

Received: February 3, 2009

Revised: June 5, 2009

Accepted: August 10, 2009

Published: September 1, 2009

REFERENCES

- Apovian, C.M., Bigornia, S., Mott, M., Meyers, M.R., Ullor, J., Gagua, M., McDonnell, M., Hess, D., Joseph, L., and Gokce, N. (2008). Adipose macrophage infiltration is associated with insulin resistance and vascular endothelial dysfunction in obese subjects. *Arterioscler. Thromb. Vasc. Biol.* 28, 1654–1659.
- Bar-Sagi, D., and Hall, A. (2000). Ras and Rho GTPases: a family reunion. *Cell* 103, 227–238.
- Camenisch, G., Pisabarro, M.T., Sherman, D., Kowalski, J., Nagel, M., Hass, P., Xie, M.H., Gurney, A., Bodary, S., Liang, X.H., et al. (2002). ANGPTL3 stimulates endothelial cell adhesion and migration via integrin α v β 3 and induces blood vessel formation in vivo. *J. Biol. Chem.* 277, 17281–17290.
- DeFronzo, R.A., Tobin, J.D., and Andres, R. (1979). Glucose clamp technique: a method for quantifying insulin secretion and resistance. *Am. J. Physiol.* 237, E214–E223.
- Dormond, O., Foletti, A., Paroz, C., and Ruegg, C. (2001). NSAIDs inhibit α v β 3 integrin-mediated and Cdc42/Rac-dependent endothelial-cell spreading, migration and angiogenesis. *Nat. Med.* 7, 1041–1047.
- Dvorak, H.F., Senger, D.R., Dvorak, A.M., Harvey, V.S., and McDonagh, J. (1985). Regulation of extravascular coagulation by microvascular permeability. *Science* 227, 1059–1061.
- Eckel, R.H., Grundy, S.M., and Zimmet, P.Z. (2005). The metabolic syndrome. *Lancet* 365, 1415–1428.
- Friedl, P., and Weigelin, B. (2008). Interstitial leukocyte migration and immune function. *Nat. Immunol.* 9, 960–969.
- Fryer, B.H., and Field, J. (2005). Rho, Rac, Pak and angiogenesis: old roles and newly identified responsibilities in endothelial cells. *Cancer Lett.* 229, 13–23.
- Graves, K.L., and Roman, J. (1996). Fibronectin modulates expression of inter-leukin-1 β and its receptor antagonist in human mononuclear cells. *Am. J. Physiol.* 271, L61–L69.
- Hato, T., Tabata, M., and Oike, Y. (2008). The role of angiopoietin-like proteins in angiogenesis and metabolism. *Trends Cardiovasc. Med.* 18, 6–14.
- Herrick, S., Blanc-Brude, O., Gray, A., and Laurent, G. (1999). Fibrinogen. *Int. J. Biochem. Cell Biol.* 31, 741–746.

- Hosogai, N., Fukuhara, A., Oshima, K., Miyata, Y., Tanaka, S., Segawa, K., Furukawa, S., Tochino, Y., Komuro, R., Matsuda, M., and Shimomura, I. (2007). Adipose tissue hypoxia in obesity and its impact on adipocytokine dysregulation. *Diabetes* 56, 901–911.
- Hynes, R.O. (2002). Integrins: bidirectional, allosteric signaling machines. *Cell* 110, 673–687.
- Ito, Y., Oike, Y., Yasunaga, K., Hamada, K., Miyata, K., Matsumoto, S., Sugano, S., Tanihara, H., Masuho, Y., and Suda, T. (2003). Inhibition of angiogenesis and vascular leakiness by angiopoietin-related protein 4. *Cancer Res.* 63, 6651–6657.
- Jackson, J.R., Seed, M.P., Kircher, C.H., Willoughby, D.A., and Winkler, J.D. (1997). The codependence of angiogenesis and chronic inflammation. *FASEB J.* 11, 457–465.
- Kadowaki, T., and Yamauchi, T. (2005). Adiponectin and adiponectin receptors. *Endocr. Rev.* 26, 439–451.
- Kanda, H., Tateya, S., Tamori, Y., Kotani, K., Hiasa, K., Kitazawa, R., Kitazawa, S., Miyachi, H., Maeda, S., Egashira, K., and Kasuga, M. (2006). MCP-1 contributes to macrophage infiltration into adipose tissue, insulin resistance, and hepatic steatosis in obesity. *J. Clin. Invest.* 116, 1494–1505.
- Kim, I., Moon, S.O., Koh, K.N., Kim, H., Uhm, C.S., Kwak, H.J., Kim, N.G., and Koh, G.Y. (1999). Molecular cloning, expression, and characterization of angiopoietin-related protein. angiopoietin-related protein induces endothelial cell sprouting. *J. Biol. Chem.* 274, 26523–26528.
- Klein, S., de Fougères, A.R., Blaikie, P., Khan, L., Pepe, A., Green, C.D., Kotliansky, V., and Giancotti, F.G. (2002). Alpha 5 beta 1 integrin activates an NF-kappa B-dependent program of gene expression important for angiogenesis and inflammation. *Mol. Cell. Biol.* 22, 5912–5922.
- Kubota, Y., Oike, Y., Satoh, S., Tabata, Y., Niikura, Y., Morisada, T., Akao, M., Urano, T., Ito, Y., Miyamoto, T., et al. (2005a). Cooperative interaction of Angiopoietin-like proteins 1 and 2 in zebrafish vascular development. *Proc. Natl. Acad. Sci. USA* 102, 13502–13507.
- Luster, A.D., Alon, R., and von Andrian, U.H. (2005). Immune cell migration in inflammation: present and future therapeutic targets. *Nat. Immunol.* 6, 1182–1190.
- Matthews, D.R., Hosker, J.P., Rudenski, A.S., Naylor, B.A., Treacher, D.F., and Turner, R.C. (1985). Homeostasis model assessment: insulin resistance and beta-cell function from fasting plasma glucose and insulin concentrations in man. *Diabetologia* 28, 412–419.
- McDonald, D.M. (1994). Endothelial gaps and permeability of venules in rat tracheas exposed to inflammatory stimuli. *Am. J. Physiol.* 266, L61–L83.
- Mettouchi, A., Klein, S., Guo, W., Lopez-Lago, M., Lemichez, E., Westwick, J.K., and Giancotti, F.G. (2001). Integrin-specific activation of Rac controls progression through the G(1) phase of the cell cycle. *Mol. Cell* 8, 115–127.
- Mokdad, A.H., Ford, E.S., Bowman, B.A., Dietz, W.H., Vinicor, F., Bales, V.S., and Marks, J.S. (2003). Prevalence of obesity, diabetes, and obesity-related health risk factors, 2001. *JAMA* 289, 76–79.
- Mosesson, M.W. (2005). Fibrinogen and fibrin structure and functions. *J. Thromb. Haemost.* 3, 1894–1904.
- Neels, J.G., and Olefsky, J.M. (2006). Inflamed fat: what starts the fire? *J. Clin. Invest.* 116, 33–35.
- Nishimura, S., Manabe, I., Nagasaki, M., Seo, K., Yamashita, H., Hosoya, Y., Ohsugi, M., Tobe, K., Kadowaki, T., Nagai, R., and Sugiura, S. (2008). In vivo imaging in mice reveals local cell dynamics and inflammation in obese adipose tissue. *J. Clin. Invest.* 118, 710–721.
- Oike, Y., Yasunaga, K., and Suda, T. (2004). Angiopoietin-related/angiopoietin-like proteins regulate angiogenesis. *Int. J. Hematol.* 80, 21–28.
- Oike, Y., Akao, M., Kubota, Y., and Suda, T. (2005a). Angiopoietin-like proteins: potential new targets for metabolic syndrome therapy. *Trends Mol. Med.* 11, 473–479.
- Oike, Y., Akao, M., Yasunaga, K., Yamauchi, T., Morisada, T., Ito, Y., Urano, T., Kimura, Y., Kubota, Y., Maekawa, H., et al. (2005b). Angiopoietin-related growth factor antagonizes obesity and insulin resistance. *Nat. Med.* 11, 400–408.
- Perona, R., Montaner, S., Saniger, L., Sanchez-Perez, I., Bravo, R., and Lacal, J.C. (1997). Activation of the nuclear factor-kappaB by Rho, CDC42, and Rac-1 proteins. *Genes Dev.* 11, 463–475.
- Roman, J., Ritzenthaler, J.D., Boles, B., Lois, M., and Roser-Page, S. (2004). Lipopolysaccharide induces expression of fibronectin alpha 5 beta 1-integrin receptors in human monocytic cells in a protein kinase C-dependent fashion. *Am. J. Physiol. Lung Cell. Mol. Physiol.* 287, L239–L249.
- Rose, D.M., Alon, R., and Ginsberg, M.H. (2007). Integrin modulation and signaling in leukocyte adhesion and migration. *Immunol. Rev.* 218, 126–134.
- Schenk, S., Saberi, M., and Olefsky, J.M. (2008). Insulin sensitivity: modulation by nutrients and inflammation. *J. Clin. Invest.* 118, 2992–3002.
- Sulciner, D.J., Irani, K., Yu, Z.X., Ferrans, V.J., Goldschmidt-Clermont, P., and Finkel, T. (1996). rac1 regulates a cytokine-stimulated, redox-dependent pathway necessary for NF-kappaB activation. *Mol. Cell. Biol.* 16, 7115–7121.
- Weisberg, S.P., Hunter, D., Huber, R., Lemieux, J., Slaymaker, S., Vaddi, K., Charo, I., Leibel, R.L., and Ferrante, A.W., Jr. (2006). CCR2 modulates inflammatory and metabolic effects of high-fat feeding. *J. Clin. Invest.* 116, 115–124.
- Ye, J. (2009). Emerging role of adipose tissue hypoxia in obesity and insulin resistance. *Int. J. Obes.* 33, 54–66.

Zyxin Mediates Actin Fiber Reorganization in Epithelial–Mesenchymal Transition and Contributes to Endocardial Morphogenesis

Masaki Mori,* Hironori Nakagami,* Nobutaka Koibuchi,[†] Koichi Miura,[‡] Yoichi Takami,* Hiroshi Koriyama,* Hiroki Hayashi,* Hisataka Sabe,[§] Naoki Mochizuki,[‡] Ryuichi Morishita,^{||} and Yasufumi Kaneda*

*Division of Gene Therapy Science and ^{||}Department of Clinical Gene Therapy, Graduate School of Medicine, Osaka University, Osaka 565-0871, Japan; [†]Department of Advanced Clinical Science and Therapeutics, University of Tokyo, Tokyo 113-8656, Japan; [‡]Department of Structural Analysis, National Cardiovascular Center Research Institute, Osaka 565-8565, Japan; and [§]Department of Molecular Biology, Osaka Bioscience Institute, Osaka 565-0874, Japan

Submitted January 15, 2009; Revised April 27, 2009; Accepted May 4, 2009
Monitoring Editor: Asma Nusrat

Epithelial–mesenchymal transition (EMT) confers destabilization of cell–cell adhesion and cell motility required for morphogenesis or cancer metastasis. Here we report that zyxin, a focal adhesion-associated LIM protein, is essential for actin reorganization for cell migration in TGF- β 1-induced EMT in normal murine mammary gland (NMuMG) cells. TGF- β 1 induced the relocation of zyxin from focal adhesions to actin fibers. In addition, TGF- β 1 up-regulated zyxin via a transcription factor, Twist1. Depletion of either zyxin or Twist1 abrogated the TGF- β 1-dependent EMT, including enhanced cell motility and actin reorganization, indicating the TGF- β 1–Twist1–zyxin signal for EMT. Both zyxin and Twist1 were predominantly expressed in the cardiac atrioventricular canal (AVC) that undergoes EMT during heart development. We further performed *ex vivo* AVC explant assay and revealed that zyxin was required for the reorganization of actin fibers and migration of the endocardial cells. Thus, zyxin reorganizes actin fibers and enhances cell motility in response to TGF- β 1, thereby regulating EMT.

INTRODUCTION

Epithelial–mesenchymal transition (EMT) is an essential event during embryogenesis for the formation of many tissues including the mesoderm, for migration of neural crest cells, and for development of the heart valves and septa. The picture emerging from diverse EMT-related studies suggests that precise molecular and cellular control of EMT is complex and context-dependent (Nakaya *et al.*, 2008). An example of developmentally regulated EMT occurs during the initial stages of cardiac morphogenesis. At embryonic day 9.5 (E9.5), endocardial cells undergo EMT (“endocardial EMT”); delaminating from the endothelial sheet, invading the matrix tissue called cardiac jelly, and engaging in endocardial cushion cellularization required for valve and septum formation (Chang *et al.*, 2004). Because a number of congenital heart diseases are caused by abnormal atrioventricular canal (AVC) development (Bruneau, 2008), understanding of the molecular basis of AVC morphogenesis has

been long sought, but still not fully achieved. Several EMT-inducing transcription factors such as Snail (Cano *et al.*, 2000) and Twist1 (Ma *et al.*, 2005) are expressed in endocardium during development. Although among them, Twist1 is well analyzed as a potent EMT inducer during cancer metastasis (Yang *et al.*, 2004); however, the role for Twist1 in AVC development is not fully understood.

An important hallmark of EMT is an increase in cell motility with actin cytoskeletal rearrangement. On EMT induction, the structure of actin cytoskeleton changes dynamically from cortical actin network to stress fiber (Zavadil and Bottinger, 2005). Cell motility also depends on the adhesion of the cell to the substratum where the integrin family molecules bind to the extracellular matrix to form focal adhesion complexes. Stress fibers link the focal adhesion to retract the cells. Furthermore, the nascent focal complexes at the leading edge of the migrating cells are needed for cell crawling by connecting the actin fibers between the front and rear focal adhesions. Thus, coordinated control of the various focal adhesion proteins is important for actin fiber reorganization. Among focal adhesion molecules, paxillin, focal adhesion kinase (FAK) and Hic-5 are reported to be involved in EMT (Hetey *et al.*, 2005; Tumbarello *et al.*, 2005). EMT induction in normal murine mammary gland (NMuMG) cells by TGF- β 1 induces the phosphorylation and recruitment of paxillin to focal adhesions and the expression of Hic-5 (Tumbarello *et al.*, 2005).

Transforming growth factor β (TGF- β) is a potent EMT inducer and is implicated in a broad kind of EMT in cancer

This article was published online ahead of print in *MBC in Press* (<http://www.molbiolcell.org/cgi/doi/10.1091/mbc.E09-01-0046>) on May 13, 2009.

Address correspondence to: Hironori Nakagami (nakagami@gts.med.osaka-u.ac.jp) or Yasufumi Kaneda (kaneday@gts.med.osaka-u.ac.jp).

Abbreviations used: AVC, atrioventricular canal; EMT, epithelial–mesenchymal transition; NMuMG, normal murine mammary gland.

metastasis, tissue fibrosis, or tissue morphogenesis (Zavadil and Bottinger, 2005). TGF- β was first described as an inducer of EMT in normal mammary epithelial cells (Miettinen *et al.*, 1994), and murine mammary epithelial cells treated with TGF- β undergo a complete EMT (Thiery, 2003). Accumulating evidences revealed the involvement of TGF- β in vital steps during development (Sanford *et al.*, 1997; Bartram *et al.*, 2001; Sridurongrit *et al.*, 2008).

Zyxin belongs to a LIM protein family and harbors distinct actin polymerization activity independent of the Arp2/3 complex (Fradelizi *et al.*, 2001). Zyxin has three tandem LIM domains in its C terminus that support specific protein interactions (Schmeichel and Beckerle, 1994) and targeting to focal adhesions (Nix *et al.*, 2001). The proline-rich N-terminal domain called ActA mediates actin polymerization (Fradelizi *et al.*, 2001). Zyxin locates primarily at focal adhesions and regulates actin cytoskeleton dynamics, cell movement, and signal transduction (Beckerle, 1998; Kadmas and Beckerle, 2004). Despite the understanding of zyxin, its role in the cellular actin rearrangement and its function *in vivo* is still unknown. A role for zyxin during development also remains to be elucidated.

In this study, we investigated the function of zyxin in TGF- β 1-induced EMT and the EMT during heart morphogenesis and explored the requirement of zyxin in TGF- β 1-dependent EMT and the contribution of zyxin to EMT for valvulogenesis in the heart.

Here, we show that zyxin regulates EMT by accelerating cell motility through controlling actin fiber reorganization in cultured epithelial cells and the endocardial cells of the embryonic heart.

MATERIALS AND METHODS

Cell Culture

NMuMG cells were obtained from ATCC (Manassas, VA) and maintained in DMEM supplemented with 10% FCS and 10 μ g/ml insulin. We cloned the cells by limiting dilution and obtained 13 different clones. Among them, we used a cell line designated C7 that showed typical epithelial morphology and robust response to TGF- β 1. The cells were maintained in DMEM (Nacalai Tesque, Tokyo, Japan) supplemented with 10% fetal bovine serum (FBS). TGF- β 1-stimulation experiments were performed with recombinant human TGF- β 1 (2 ng/ml; R&D Systems, Minneapolis, MN).

Deletion Mutants and Retroviral Vector Construction

Zyxin deletion mutants were generated by PCR amplifying the amino acid 1-375 (Δ LIM) or aa 376-564 (LIM only) region and inserting into pCAGIP-EGFP (enhanced green fluorescent protein) vector.

pCX4 puro vector was kindly provided by Tsuyoshi Akagi (Akagi *et al.*, 2003). pCX4 puro-EGFP-Snail, pCX4 puro-EGFP-Twist1, or pCX4 puro-HMGA2 were generated by inserting the full-length Snail cDNA from pCAGGS-EGFP-Snail, Twist1 cDNA from pCAGIP-Twist1 (Hayashi *et al.*, 2007), or HMGA2 cDNA from pENTR-HMGA2 into the pCX4 puro vector, respectively. Each plasmid above was cotransfected with pGP and pE-co (Takara Bio, Tokyo, Japan) into BOSCO to produce ecotropic retrovirus vector.

Immunocytochemistry

NMuMG-C7 cells were plated onto collagen-coated glass-bottom dishes (MatTek, Ashland, MA). The cells were fixed in 4% paraformaldehyde (PFA), permeabilized in 0.1% Triton X-100 for 5 min, and probed with mouse anti-zyxin antibody (1:40, 164D4, Synaptic Systems; 1:100, clone ZOL301, Sigma-Aldrich, St. Louis, MO), mouse anti-E-cadherin antibody (1:50, clone 36, BD Biosciences, San Jose, CA), mouse anti-N-cadherin antibody (1:50, clone 32, BD Biosciences), and rabbit anti-ZO-1-antibody (1:100, 61-7300, Invitrogen, Carlsbad, CA). The primary antibody was detected by goat anti-mouse-Alexa 488, goat anti-mouse-Alexa 546, or goat anti-rabbit-Alexa 546 (1:1000, Invitrogen). Nuclei were stained with 4'-6-diamidino-2-phenylindole (DAPI, Invitrogen). F-actin was stained with Alexa Fluor 546-phalloidin (Invitrogen).

Fluorescence Imaging

NMuMG-C7 cells were stably transfected with pCAGIP-EGFP-zyxin plasmid. Fluorescence images were recorded with a Nikon eclipse TE300 inverted

microscope (Melville, NY) or with a confocal microscope with a Bio-Rad laser scanning system (Radiance 2100; Richmond, CA) coupled to a Nikon eclipse TE2000-U inverted microscope with a 60 \times oil immersion objective lens. For time-lapse recording of zyxin images, the cells were grown in 35-mm glass-bottom dishes (MatTek) and placed in a CO₂ chamber (Model CZI-3; Zeiss) at 37°C, attached to the stage of an inverted microscope (Axiovert 200; Zeiss). Images were acquired every 3 min using a 40 \times 1.3 NA objective lens (Plan-NEOFLUAR, Zeiss) and a CCD camera (model HRm; Zeiss), and analyzed using Axiovision software (version 4.6, Zeiss).

SDS-PAGE and Western Blot Analysis

Cells were harvested in a RIPA lysis buffer. Protein concentration was determined by the method of Lowry (Lowry *et al.*, 1951). Protein samples (10 μ g per lane) were separated by SDS-PAGE and transferred to a Hybond-P PVDF membrane (GE Healthcare, Little Chalfont, Buckinghamshire, England). Western blot was performed with the following antibodies: anti-zyxin (1:1000, ZOL301, Sigma-Aldrich), anti-vinculin (1:1000, V9264), anti- β -actin (1:5000, AC-15), anti-E-cadherin (1:5000, clone 36, BD Biosciences), anti-N-cadherin (1:5000, clone 32), anti-paxillin (1:1000, clone 165), anti-FAK (1:200, clone 77), anti-p130Cas (1:1000, clone 21), anti-Hic-5 (1:200, clone 34), anti-GFP (1:1000, 598, MBL, Nagoya, Japan), anti-HMGA2 (1:200, ab41878, Abcam, Cambridge, MA) and anti-GAPDH (1:5000, 6C5). All secondary antibodies were horseradish peroxidase conjugated (GE Healthcare) and were used at 1:1000 dilution. Immunoreactive bands were detected with Chemi-LumiOne L (Nacalai Tesque). Quantification was done by densitometry using ImageJ software (NIH; <http://rsb.info.nih.gov/ij/>).

Modified Boyden's Chamber Assay

Modified Boyden's chamber assay was carried out as previously described (Saito *et al.*, 2006). Briefly, 27 μ l DMEM with 10% FBS was added to the lower chamber, and 50 μ l of cell suspension (5×10^5 cells/ml) in DMEM with 10% FBS was added to the upper chamber. After 4 h of incubation, the cells on the lower side of the membrane were stained with Diff-Quick (Sysmex, Hyogo, Japan) to facilitate visualization and counting of cells. The count was done in eight randomly chosen fields.

RNA Interference Experiments

Zyxin or Twist1 Stealth small interfering RNA (siRNA) oligonucleotides were purchased from Invitrogen. The double-strand RNA (dsRNA) oligonucleotides against zyxin were as follows: (sense) 5'-AACAAUUGAGUCUGCAACUGUGGG-3' and (antisense) 5'-CCCACCAGUUGCCACUCCAUUUGUU-3'. The dsRNA oligonucleotides against Twist1 were as follows: (sense) 5'-UUGAGGGUCUGAAUCUUGUCUAGCU-3' and (antisense) 5'-ACGUGAGCAAGAUUCAGACCCUCA-3'. The scrambled siRNA oligonucleotides were as follows: (sense) 5'-UUCCUCAAUAGUCCGUGUTT-3' and (antisense) 5'-ACACGCAUCUAUUGAGCAATT-3'. These sequences did not correspond to any sequence in the mouse genome when subjected to a BLAST search. Transfections were carried out using Lipofectamine 2000 (Invitrogen), according to the manufacturer's instructions.

RT-PCR Analysis and Real-Time PCR Quantification

Total RNA was isolated using an RNeasy RNA isolation kit (QIAGEN, Valencia, CA). cDNA was synthesized using High Capacity cDNA Reverse Transcription Kit (Applied Biosystems, Foster City, CA). The sequences of PCR primers are shown in the Supplementary Table S1. The reactions were performed as follows: 98°C for 30 s; 25 cycles of 98°C for 10 s, 52°C for 30 s, and 72°C for 60 s. PCR products were separated in a 1.5% agarose gel. Real-time PCR was performed using an Applied Biosystems 7900 HT Fast Real-Time PCR system with TaqMan Probe for zyxin (Mm00496120_m1) and GAPDH (Mm99999915_g1) and TaqMan Universal PCR Master Mix (Applied Biosystems). The reactions were incubated at 95°C for 10 min followed by 40 cycles of 95°C for 15 s and 60°C for 1 min. The relative expression level was calculated from a standard curve obtained by using log dilutions of cDNA containing the gene of interest. The average of two independent analyses for each gene and sample was calculated and was normalized to the endogenous reference control gene GAPDH.

In Situ Hybridization

In situ hybridization was performed as previously described (Koibuchi and Chin, 2007). The cDNAs used for generation of Dig-labeled mouse riboprobes were zyxin (nucleotides 2002-2404; GenBank no. NM_011777) and Twist1 (nucleotides 644-1524; GenBank no. NM_011658).

Lentivirus Vector

pcDNA6.2-shZyxin and pcDNA6.2-shLacZ were generated by inserting the oligonucleotide containing the specific siRNA target sequence into pcDNA6.2 vector (Invitrogen). pLenti6-shZyxin and pLenti6-shLacZ were generated from pcDNA6.2 constructs. Lentivirus was generated by cotransfection of the above construct with packaging plasmids into 293FT cells according to the

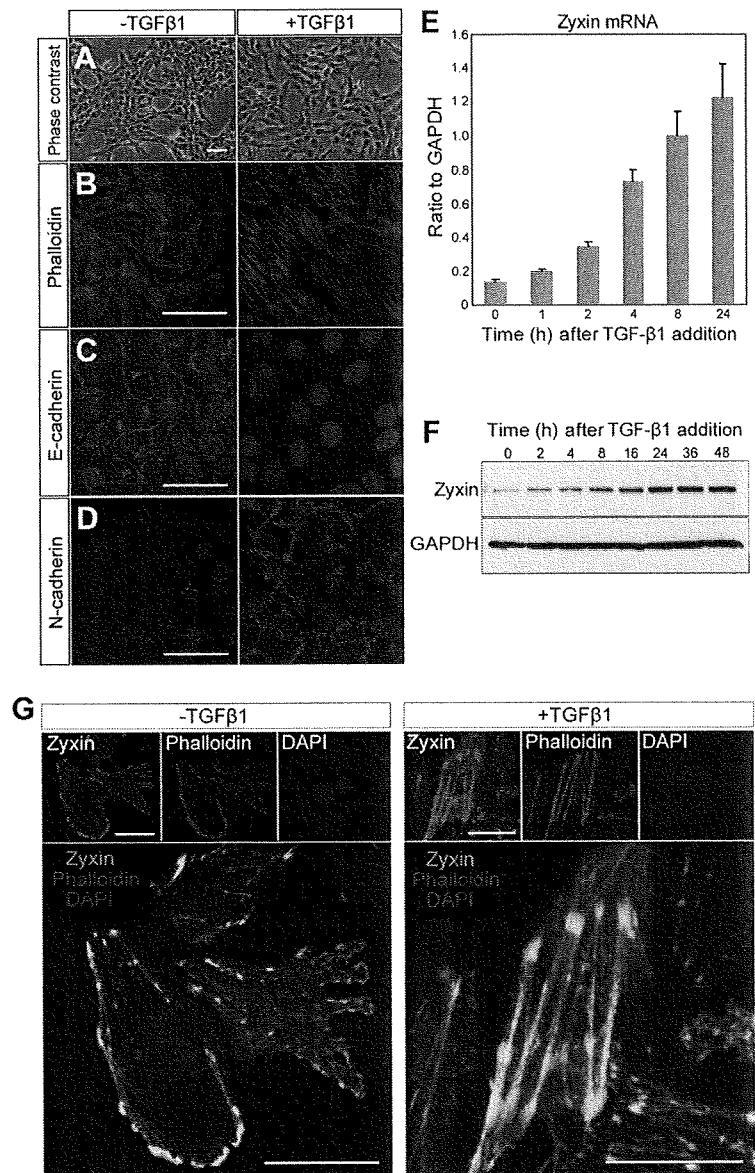


Figure 1. Zyxin is up-regulated and relocates to actin stress fibers in TGF-β1-induced EMT. (A–D) TGF-β1-induced in vitro EMT in NMuMG-C7 cells. NMuMG-C7 cells treated with TGF-β1 for 24 h exhibit the cell scattering (A), actin stress fiber formation (B), down-regulation of E-cadherin (C), and up-regulation of N-cadherin (D). Scale bars, 100 μm. (E) Real-time PCR analysis of zyxin mRNA in NMuMG-C7 cells treated with TGF-β1. Results are shown as the mean ± SEM (n = 3). (F) Immunoblot analysis of zyxin in NMuMG-C7 cells treated with TGF-β1. GAPDH was used as a loading control. (G) TGF-β1 induced zyxin relocation from focal adhesions to actin fibers. Confocal microscopy of EGFP-tagged zyxin (green) in NMuMG-C7 cells treated or not with TGF-β1 for 24 h. Zyxin locates at focal adhesions before TGF-β1 treatment and mobilizes to actin fibers after the treatment (Also see Supplementary Video 1). The cells were counterstained with phalloidin (red) and DAPI (blue). Scale bars, 50 μm.

manufacturer’s instruction (Invitrogen). The sequences of shZyxin DNA oligo and shLacZ control oligo are available in the Supplementary Table SII.

Ex Vivo EMT Assay

The experiments were approved by the Ethics Committee for Animal Experiments of Osaka University Graduate School of Medicine. C57BL/6 mice were purchased from Charles River Breeding Laboratories. The ex vivo EMT assay was performed as described (Camenisch *et al.*, 2002) with some modifications. After putting E9.5 AVC explants on collagen gels, lentivirus-containing medium was added and incubated for 24 h. Then the explants were incubated with M199 media (Invitrogen/BRL, Rockville, MD) supplemented with 0.01% insulin, transferrin and selenium (ITS, Invitrogen/BRL) for 48 h, before determining the extent of outgrowth and matrix invasion. The criteria for “Migratory” were the appearance of the stellate cells migrating outward, frequently invading the collagen gel matrix. The criteria for “Nonmigratory” were the appearance of polygonal cells that form cobblestone-like colonies on the gel surface (Camenisch *et al.*, 2002). XZ confocal images were acquired to visualize collagen gel invasion. Cells that migrated into the collagen gel were stained with DAPI and counted in randomly collected areas. Phalloidin staining of the explants was done after the fixation with 4% PFA for 20 min on the collagen gel.

Statistics

Statistical analysis was performed with StatView 5.0 software (SAS Institute, Cary, NC). All results were expressed as mean ± SEM. Data were compared using ANOVA, followed by the Dunnett test for pairwise comparisons against control and by the Tukey test for multiple comparisons. Significance was defined as p < 0.05.

RESULTS

Zyxin Is Up-Regulated in TGF-β1-induced EMT and Mobilizes to Actin Fibers

Normal murine mammary gland (NMuMG) cells undergo EMT upon treatment with TGF-β1 (Tumbarello *et al.*, 2005). As reported, original NMuMG cells have heterogeneous morphology and responsiveness to TGF-β1. Thus, we cloned the cells by limiting dilution and established a cell line of NMuMG cells named NMuMG-C7, which altered the morphology in response to TGF-β1. On TGF-β1 treatment, NMuMG-C7 cells exhibited a series of EMT hallmarks such

as cell scattering (Figure 1A), actin stress fiber formation (Figure 1B), down-regulation of E-cadherin (Figure 1C), and up-regulation of N-cadherin (Figure 1D). We observed that TGF- β 1 up-regulated zyxin mRNA (Figure 1E) and induced expression of zyxin (Figure 1F) in a time-dependent manner, suggesting the possible participation of zyxin in TGF- β 1-dependent EMT. An increase of zyxin protein was seen as early as 2 h after treatment and was dramatically augmented later on.

To study how zyxin participates in TGF- β 1-dependent EMT, we examined the localization of zyxin using EGFP-tagged zyxin before and after the TGF- β 1 treatment. Previous reports confirmed the localization of EGFP-tagged zyxin corresponded to the endogenous zyxin (Nix *et al.*, 2001; Hotulainen and Lappalainen, 2006). Without stimulation, consistent with a previous report (Yoshigi *et al.*, 2005), zyxin localized to focal adhesions and focal complexes in the lamellipodia (Figure 1G, -TGF- β 1). Of note, upon TGF- β 1 stimulation, zyxin mobilized from focal adhesions to actin fibers (Figure 1G, +TGF- β 1). The localization of zyxin in confluent cells was shown in Supplementary Figure S1. Time-lapse imaging revealed the translocation of zyxin to actin fibers in NMuMG-C7 cells treated with TGF- β 1 (Supplementary Video 1). These findings lead us to assume the switch of the role for zyxin from the regulation of cell-extracellular matrix adhesion to that of actin fibers and suggest the involvement of zyxin in EMT.

Zyxin Is Required for Cell Migration and Actin Fiber Reorganization in EMT

To assess the requirement of zyxin in TGF- β 1-induced EMT, we performed knockdown experiments of zyxin. The effectiveness of zyxin siRNA was confirmed in NMuMG-C7 cells (Figure 2A). TGF- β 1 induced the expression of N-cadherin and reduced the expression of E-cadherin (Figure 2A). Depletion of zyxin affected the expression of neither E-cadherin nor N-cadherin and altered the localization of neither E-cadherin nor N-cadherin (Figure 2A and Supplementary Figure S2). We further assessed the effect of depletion of zyxin on TGF- β 1-dependent cell motility. Knockdown of zyxin almost completely abolished TGF- β 1-induced migration (Figure 2, B and C). These results indicate that zyxin is essential for TGF- β 1-induced migration, a hallmark of EMT. Next, we examined the effect of zyxin depletion on actin cytoskeleton by phalloidin staining. Polarized epithelial cells including NMuMG cells have distinct actin networks in the apical and the basal side of the cells (Supplementary Figure S3). The apical actin fibers adhere to adherens junctions (Yonemura *et al.*, 1995; Vasioukhin *et al.*, 2000; Perez-Moreno *et al.*, 2003) and the basal actin stress fibers adhere to focal adhesions. We found that TGF- β 1 induced both apical and basal actin fiber formation (Figure 2, E and I). Knockdown of zyxin resulted in inhibition of actin fiber formation at the basal level and, to a lesser extent, at the apical level (Figure 2, G and K). To examine how essential zyxin was in EMT, we carried out rescue experiments using EGFP-tagged zyxin mutants (Figure 2L). The endogenous zyxin was depleted with short hairpin RNA (shRNA) that targets 3' untranslated region (UTR) of zyxin mRNA (Figure 2M). The expression of exogenous zyxin mutants were confirmed (Figure 2M). The formation of actin stress fibers induced by TGF- β 1 was rescued by the expression of EGFP-tagged full-length (FL) zyxin construct, supporting the specificity of zyxin siRNA and shRNA against zyxin. To the contrary, Δ LIM mutant dispersed in cytosol and failed to rescue. LIM only mutant exhibited localization to cytosol, focal adhesions, and nuclei and failed to rescue. Zyxin has ActA sequence in

its N terminus, which has a distinct actin fiber polymerization activity (Fradelizi *et al.*, 2001), and in LIM domains, which is necessary for targeting to focal adhesions (Nix *et al.*, 2001). These experiments suggested that in the induction of EMT, both the localization and the activity were essential for zyxin. These findings suggest that zyxin is involved in TGF- β 1-dependent EMT by regulating cell migration via controlling actin fiber formation. Considering that one of the most important features of EMT is the acquisition of motility (Thiery, 2003; Sung *et al.*, 2007), Zyxin appears to be essential for the progression of EMT.

Zyxin Is Expressed in AVC of Developing Heart and Valves in Mice

We sought the physiological role for zyxin in EMT. During development, EMT occurs during AVC morphogenesis that gives rise to valves and septa. We therefore investigated the expression of zyxin during development by in situ hybridization in mouse fetus. We found that zyxin was strongly expressed in AVC at E13.5 (Figure 3A, arrowhead). We examined the expression of zyxin in more detail during development and revealed that its expression at AVC was induced during development, peaked in AVC at E13.5 and waned in valves and septa at E14.5 (Figure 3B, arrowhead). These expression patterns of zyxin prompted us to assume that zyxin was involved in the endocardial EMT and that the cells expressing zyxin contributed to valvulogenesis. We further examined the expression of Twist1 and found the concordance of the expression between Twist1 and zyxin in AVC (Figure 3B). These findings are in agreement with the in vitro results of zyxin regulation by Twist1 (see below). Furthermore, analyses in adults revealed the expression of zyxin in valves (Figure 3C, arrowhead). These findings imply that zyxin-expressing cells that undergo endocardial EMT participate in valvulogenesis.

Next, we examined whether the involvement of zyxin in TGF- β 1-EMT was similarly seen in vascular endothelial cells (Supplementary Figure S4) in vitro. TGF- β 1 induced cell scattering and actin fiber formation in murine vascular endothelial cells (Supplementary Figure S4A). Knockdown of zyxin (Supplementary Figure S4B) repressed the actin fiber formation induced by TGF- β 1 (Supplementary Figure S4C). Moreover, in bovine arterial endothelial cells, TGF- β 1 treatment induced the cell shape change into fusiform (Supplementary Figure S4D) and up-regulation of zyxin (Supplementary Figure S4E).

Zyxin Is Required for Morphogenetic Movement of the Endocardial Cells

To understand how zyxin regulates EMT in the endocardial cells, we performed an ex vivo EMT assay (Figure 4A). The AVC explants isolated from E9.5 embryos recapitulate the process of EMT extracorporeally (Runyan and Markwald, 1983). We generated lentivirus vector expressing either zyxin shRNA or control LacZ shRNA to evaluate the effect of loss of zyxin expression in endocardial EMT. The efficacy of knockdown was confirmed after zyxin shRNA transduction (Figure 4B). The transduction efficiency was more than 85% by the estimation on the basis of EGFP fluorescence coexpressed on a single transcript (Figure 4C). The explants transduced with control shLacZ showed extensive radial migration of stellate cells with abundant protrusions (Figure 4D, LacZ shRNA). In contrast, the explants transduced with shZyxin showed significantly reduced cell migration and exhibited cobblestone-like appearance composed of polygonal cells (Figure 4D, zyxin shRNA). Although 76% of the explants transduced with shLacZ showed robust outgrowth

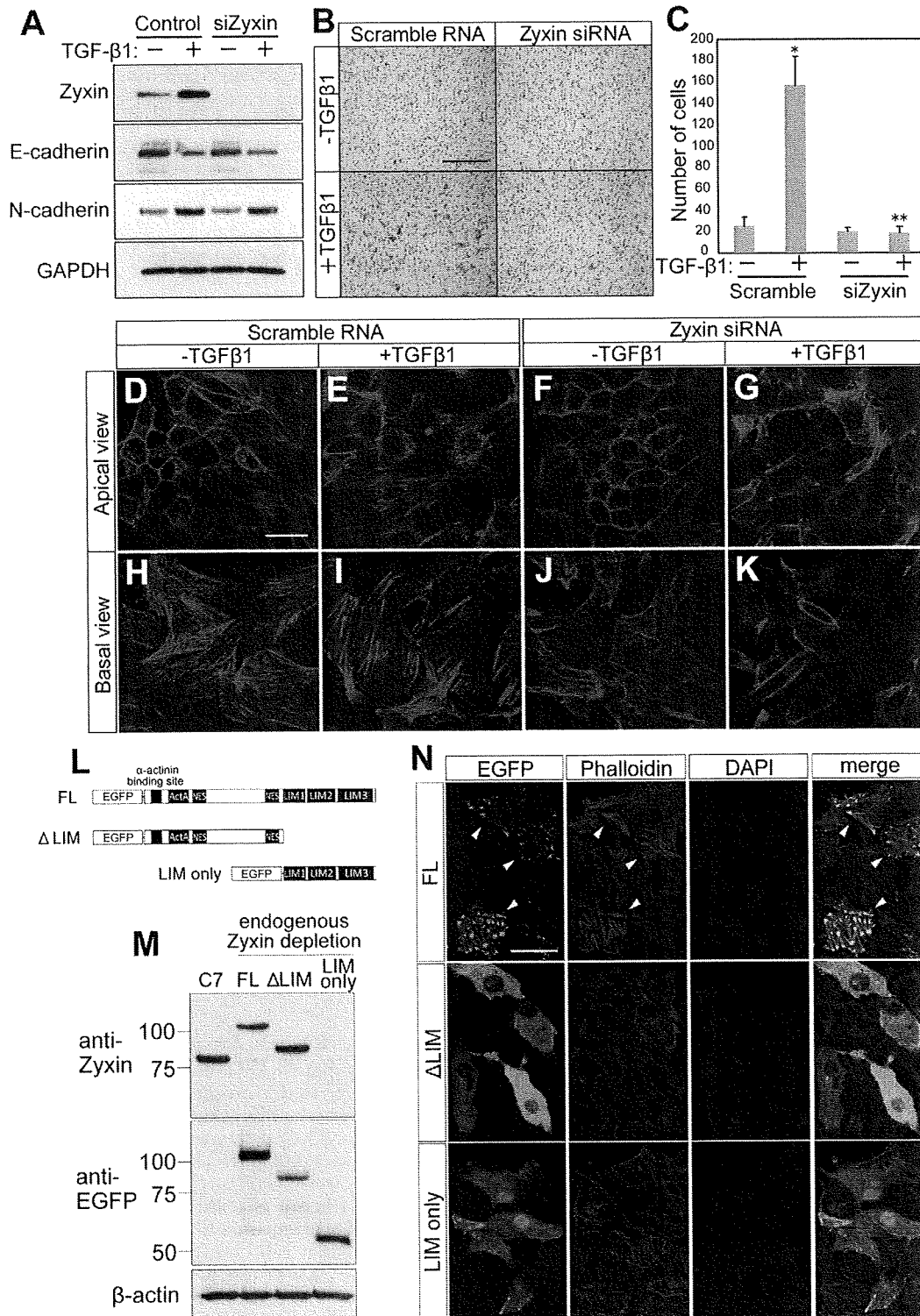


Figure 2. Zyxin is essential for cell migration and actin fiber reorganization in TGF-β1-induced EMT. (A) Immunoblot analysis of zyxin and E- and N-cadherin in NMuMG-C7 cells transfected with zyxin siRNA or scramble RNA. After treatment with TGF-β1 for 24 h, total lysates were subjected to Western blot. GAPDH was used as a loading control. (B) Zyxin depletion abolished cell motility in TGF-β1-EMT. Cell motility was assessed by modified Boyden's chamber assay. NMuMG-C7 cells were transfected with zyxin siRNA or scramble RNA and treated or not with TGF-β1 for 24 h. The cells that migrated to the lower surface of the membrane were stained after 4 h of incubation. Scale bar, 250 μm. (C) The number of migrated cells in B. *p = 0.0344 versus Scramble RNA, TGF-β1 (-); **p = 0.0159 versus Scramble RNA, TGF-β1 (+). Results are shown as the mean ± SEM of four separate migration assays from two independent experiments. (D-K) Zyxin is essential for actin fiber formation in TGF-β1-EMT. Phalloidin staining was performed with NMuMG-C7 cells transfected with zyxin siRNA